isvr Institute of Sound and Vibration Research

Studies into the Detection of Buried Objects (Particularly Optical Fibres) in Saturated Sediment. Part 2: Design and Commissioning of Test Tank

T.G. Leighton and R.C.P. Evans

ISVR Technical Report No 310

April 2007

University of Southampton

SCIENTIFIC PUBLICATIONS BY THE ISVR

Technical Reports are published to promote timely dissemination of research results by ISVR personnel. This medium permits more detailed presentation than is usually acceptable for scientific journals. Responsibility for both the content and any opinions expressed rests entirely with the author(s).

Technical Memoranda are produced to enable the early or preliminary release of information by ISVR personnel where such release is deemed to the appropriate. Information contained in these memoranda may be incomplete, or form part of a continuing programme; this should be borne in mind when using or quoting from these documents.

Contract Reports are produced to record the results of scientific work carried out for sponsors, under contract. The ISVR treats these reports as confidential to sponsors and does not make them available for general circulation. Individual sponsors may, however, authorize subsequent release of the material.

Studies into the detection of buried objects (particularly optical fibres) in saturated sediment. Part 2: Design and commissioning of test tank

T G Leighton and R C P Evans

ISVR Technical Report No. 310

April 2007

UNIVERSITY OF SOUTHAMPTON

INSTITUTE OF SOUND AND VIBRATION RESEARCH

FLUID DYNAMICS AND ACOUSTICS GROUP

Studies into the detection of buried objects (particularly optical fibres) in saturated sediment. Part 2: Design and commissioning of test tank

by

T G Leighton and R C P Evans

ISVR Technical Report No. 310

April 2007

Authorized for issue by
Professor R J Astley, Group Chairman

ACKNOWLEDGEMENTS

TGL is grateful to the Engineering and Physical Sciences Research Council and Cable & Wireless for providing a studentship for RCPE to conduct this project.

CONTENTS

FIGURE CAPTIONS

ABSTRACT

This report is the second in a series of five, designed to investigate the detection of targets buried in saturated sediment, primarily through acoustical or acoustics-related methods. Although steel targets are included for comparison, the major interest is in targets (polyethylene cylinders and optical fibres) which have a poor acoustic impedance mismatch with the host sediment. This particular report details the construction of a laboratory-scale test facility. This consisted of three main components. Budget constraints were an over-riding consideration in the design.

First, there is the design and production of a tank containing saturated sediment. It was the intention that the physical and acoustical properties of the laboratory system should be similar to those found in a real seafloor environment. Particular consideration is given to those features of the test system which might affect the acoustic performance, such as reverberation, the presence of gas bubbles in the sediment, or a suspension of particles above it. Sound speed and attenuation were identified as being critical parameters, requiring particular attention. Hence, these were investigated separately for each component of the acoustic path.

Second, there is the design and production of a transducer system. It was the intention that this would be suitable for an investigation into the non-invasive acoustic detection of buried objects. A focused reflector is considered to be the most cost-effective way of achieving a high acoustic power and narrow beamwidth. A comparison of different reflector sizes suggested that a larger aperture would result in less spherical aberration, thus producing a more uniform sound field. Diffraction effects are reduced by specifying a tolerance of much less than an acoustic wavelength over the reflector surface. The free-field performance of the transducers was found to be in agreement with the model prediction. Several parameters have been determined in this report that pertain to the acoustical characteristics of the water and sediment in the laboratory tank in the 10 – 100 kHz frequency range.

Third, there is the design and production of an automated control system was developed to simplify the data acquisition process. This was, primarily, a motor-driven position control system which allowed the transducers to be accurately positioned in the two-dimensional plane above the sediment. Thus, it was possible for the combined signal generation, data acquisition and position control process to be co-ordinated from a central computer.

This series of reports is written in support of the article “The detection by sonar of

difficult targets (including centimetre-scale plastic objects and optical fibres) buried in saturated sediment” by T G Leighton and R C P Evans, written for a Special Issue of *Applied Acoustics* which contains articles on the topic of the detection of objects buried in marine sediment. Further support material can be found at http://www.isvr.soton.ac.uk/FDAG/uaua/target_in_sand.HTM.

LIST OF SYMBOLS

A	A constant describing the amplitude of the scaler potential of a transmitted wave
a_{np}	Attenuation coefficient
B	A constant describing the decay in amplitude of the scaler potential of a transmitted wave
c_f	Speed of sound in a fluid
c_1	Phase speed of compressional acoustic waves in medium 1
c_2	Phase speed of compressional acoustic waves in medium 2
e	Exponential constant (~2.71828182)
f_k	Acoustic frequency in kilohertz
F_r	Paraxial focal length
$H(\omega)$	Frequency-domain transfer function
IL	Intensity level
I_{pa}	Pulse averaged acoustic intensity
I_{ref}	Reference acoustic intensity
j	Complex operator, $\sqrt{-1}$
$\overline{K}_b$	Complex bulk modulus of a sediment's skeletal frame
k_i	Wave number of an incident wave
k_α	An empirical constant describing the frequency dependence of attenuation.
L_0	Distance from S_0 to the rim of a spherical reflector

L_i	Distance from S_i to the rim of a spherical reflector
L_{SA}	Longitudinal spherical aberration
n	An integer, in this report for example denoting the number of equations, or estimates
n_α	An empirical constant describing the frequency dependence of attenuation.
O	Reference position of the back of a spherical reflector
OPL	Optical path length
P_{atm}	Atmospheric pressure
P_e	Effective acoustic pressure amplitude
P_g	Gauge pressure
P_{ref}	Reference effective acoustic pressure amplitude
R_{Pa}	Pressure amplitude reflection coefficient
r_r	Radius of the aperture of a spherical reflector
R_r	The principal radius of curvature of a spherical reflector
R_π	Power reflection coefficient
S_0	Separation between acoustic elements or between an acoustic element and the back of a spherical reflector (point O in figure A 1)
S_i	Distance between the point of intercept of a ray on the acoustic axis and the back of a spherical reflector (point O in figure A 1)
$S(\omega)$	Signal input to a signal processor (excluding noise)
t	Time
T	Temperature (°C)
t_g	Gauge temperature (T / 100)
T_{Pa}	Pressure amplitude transmission coefficient
T_{SA}	Transverse spherical aberration
T_π	Power transmission coefficient

x	Cartesian co-ordinate in the horizontal plane, used in this report for example to describe the distance between two hydrophones which lie in the same horizontal plane, or the horizontal coordinate direction along the interface between two media.
x_r	Depth of the aperture of a spherical reflector
x_1	Horizontal co-ordinate of measurement position 1
x_2	Horizontal co-ordinate of measurement position 2
$X(\omega)$	Frequency response of a detection system
z	The vertical Cartesian co-ordinate, in this report reflecting the penetration depth of a wave into a medium
Z	Characteristic acoustic impedance
Z_1	Characteristic acoustic impedance of medium 1
Z_2	Characteristic acoustic impedance of medium 2
α_{dB}	Attenuation coefficient
Δ	Directivity function
ϕ_r	Complementary angle, $\phi_r = (\pi - \varphi_r)$
φ_r	Angle subtended between the rim and the back of a spherical reflector
π	Pi ($\approx$ 3.141592654)
θ_c	Critical angle
θ_g	Grazing angle
θ_i	Angle of incidence
θ_r	the angle measured at the sound source and subtended between the rim of a spherical reflector and the acoustic axis
θ_t	Angle of transmission

ρ_f Density of a fluid

Σ_{LC} Diameter of the circle of least confusion

ς $\varsigma = (R_r - S_0)/L_0$ is a constant for a given spherical reflector

ω Circular frequency

ψ Acoustic wave potential

ψ_i Incident scaler acoustic wave potential

ψ_r Reflected scalar wave potential

ψ_t Transmitted scalar wave potential

ψ_x Tangential scalar wave potential along an interface (in the *x*-direction)

$\Psi(\omega)$ Frequency-domain representation of a driving signal

1 Introduction

In the previous report[1], a system based on acoustic techniques was identified as being the most likely to succeed in the direct detection of buried objects. In order to investigate this, experimentally, it was necessary to build a test facility to mimic the seabed environment. In this report, the design and construction of such a facility is described.

In the next section of this report (section 2), the physical and acoustical properties of the seabed environment are studied individually. In particular, the size and shape of the sediment material used in the test facility is examined, as well as the speed of sound and attenuation in seawater, sediment suspensions, and within the sediment. In the sub-sections that follow, these properties are compared to those found in the laboratory.

It should be noted that the acoustic path length in a field system is estimated to be up to 2 m through the water, and up to 2 m in the sediment (for the round-trip, from an ROV-mounted transducer to an object buried at a depth of up to 1 m in the sediment, and back again). A system of this size was impractical to build in the laboratory with the facilities available. Therefore, an important goal of this section was to ensure that a scaled-down version of the field environment would still give useful results.

The third section of this report deals with the transducer system. This was designed to reduce unwanted acoustic interaction with the environment, whilst increasing the likelihood of interaction with a buried object. Measurements are presented for both the free-field performance of the system, and the transmission loss within the sediment.

Section 4 briefly details the position control system which guided the transducers within the tank. Under the direction of a single computer, the laboratory apparatus formed a completely automated signal generation, data acquisition and position control system.

---

[1] T G Leighton and R C P Evans, Studies into the detection of buried objects (particularly optical fibres) in saturated sediment. Part 1: Background. *ISVR Technical Report No.* 309 (2007).

2 The Test Facility

A large steel tank (150 cm × 180 cm × 125 cm deep) was obtained for the purpose of creating an acoustic test facility. It was mounted on a series of wooden blocks to reduce vibration-induced background noise. The tank was part-filled with a sediment-like material to a depth of 50 cm, and water to give a total fill-depth of 116 cm. The physical nature of the sediment and the acoustic behaviour of the water and sediment media are considered in the next two sections. Important properties are summarised in section 2.3, and the implications for the design of an acoustic detection system are discussed.

2.1 The Sediment Bed

At a sea depth of 1 000 m the seabed is, typically, composed of fine sand and clay-silt, with a mean particle diameter of less than 100 microns [1]. To reproduce 'at-sea' acoustic conditions in the laboratory tank, it was important to ensure that the composition of the artificial sediment was similar to a real seabed. A favoured laboratory material is round-grained quartz sand, which has less rigidity and attenuation than angular-grained natural sands [2]. Alternatives such as spherical particles were also considered [3] but were found to be too expensive to be used in large quantities.

For the large quantity of sediment that was required, the most convenient and cost-effective material was found to be ordinary builder's sand. The sand used conformed to the British Standard, BS 1200; a standard that specifies the process of sieving which controls the particle size distribution. (The distribution of sand grains was subsequently measured directly using a laser light scattering technique. This is presented in detail in section 2.1.2).

An important issue that had to be addressed *before* any sediment material was added to the test facility was that of bubble entrainment. In previous experiments on acoustic absorption in sand and soil [4], researchers have observed that the presence of small quantities of air can give rise to very large attenuation coefficients (74 dB cm^{-1} at 35 kHz). Thus, it was considered important to ensure that adequate steps were taken to minimise the number of air bubbles trapped within the sediment. Details of the preventative measures that were taken are presented in section 2.1.1.

In total, 2400 kg of sand was stirred into the laboratory tank, already half-filled with tap water, to achieve a fill-depth of 50 cm. The density of a sample of individual sand grains was measured to be 2 670 kg m^{-3} ± 2.5 %. (For convenience, the commonly accepted value of 2 650 kg m^{-3}, the density of quartz [5], was used in calculations.) The density of water was taken to be 1 000 kg m^{-3} with an uncertainty of ± 0.1 %, arising mainly through temperature variations. From these values, the bulk density of the water-saturated sediment was calculated to be 2 110 kg m^{-3} ± 2.5 %. (The porosity was also calculated using these values and was found to be, roughly, 0.33. This is typical of the porosities measured in sediments of this type [6].)

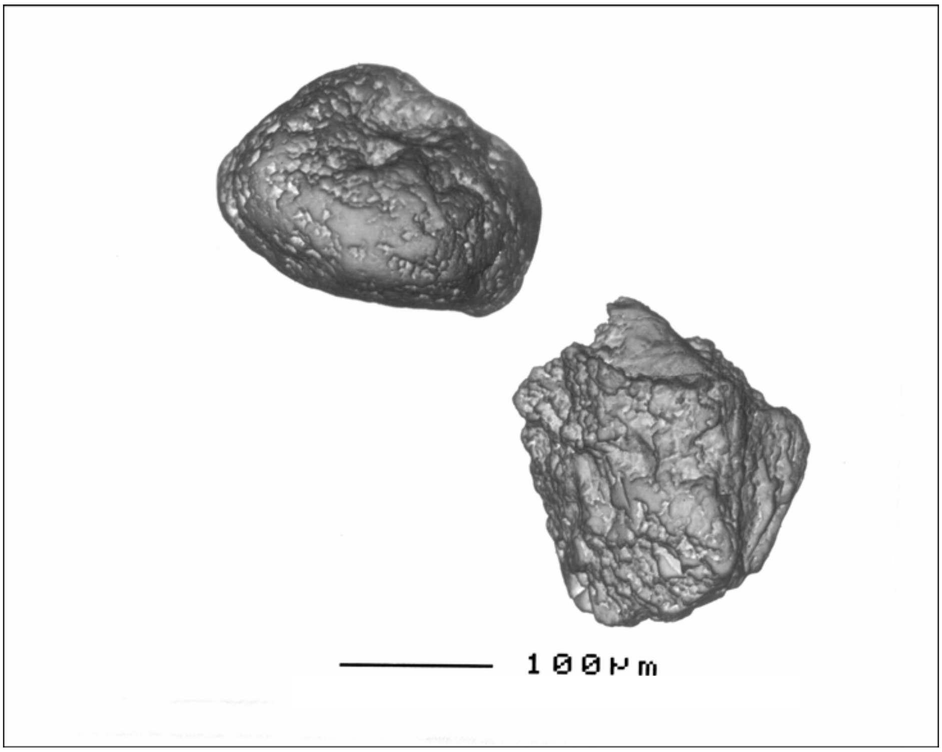

Figure 1 *A scanning electron microscope picture of two typical sand grains taken from the sediment bed. The scale bar is 100 μm in length.*

A scanning electron microscope[2] (SEM) image of some typical sand particles is presented in figure 1. The SEM was able to resolve surface topography to within 3.5 nm and could perform microanalysis and element distribution mapping with a spatial resolution of around 5 nm. Microanalysis showed the particles to be principally composed of silicon and oxygen, as expected. The angular surface features on the grains should be noted. These crevices are ideally suited for trapping pockets of air and can act as nucleation points for the generation of bubbles which may then pass into the body of the sediment [7].

2.1.1 Bubble Entrainment

Perhaps the greatest single problem with experiments involving water-saturated sediments comes from the entrainment of bubbles [2]. Gas bubbles do not present a problem at a sea depth of 1 000 m as the rate of biological out-gassing is very low. The deposition rate of silt from dead organic matter, plankton, *etc.*, is between 0.1 mm and 10 mm every 1 000 years [8]. In the laboratory, however, the inclusion of bubbles is inevitable.

Consider the dry sand which was added to the water in the laboratory tank. It has been noted that irregularities on the surfaces of individual sand grains could have trapped pockets of air that would have formed bubbles. By allowing the sediment to settle out, some bubbles would have detached themselves naturally. However, without active removal, a population of bubbles would have remained and, under the influence of diurnal temperature variations, even more bubbles would have formed [7].

Several methods of bubble removal were considered. These included: the initial entrainment of less air by using smooth, spherical particles [3]; the evacuation of air from the sediment by using a vacuum chamber [4]; and the acquisition of real, bubble-free sediment. Each of the above methods was excluded for reasons of cost or difficulty of implementation. An alternative method, the removal of bubbles by fluidising the sediment (*i.e.,* by directly agitating the sand grains) was chosen as the most practical and economical solution.

---

[2] Access to the JEOL JSM-6400 Analytical Scanning Electron Microscope used in this investigation was provided by the University of Southampton, Science and Engineering Electron Microscopy Centre.

The principle of a ‘fluidised bed’ [9] is well understood and such systems have been used in the chemical industry for a long time. If a granular material is poured into a container the surface becomes inclined at the angle of pouring. This is referred to as a ‘fixed bed’ [9]. If a fluid stream, gas or liquid, is passed upwards through the bed at a sufficient velocity, such that the force resisting the flow is equal to the bed weight, it becomes suspended and expands. Adjacent particles become mobile and the surface levels itself like a fluid. It is for this reason that the bed is said to be fluidised.

For the purpose of removing bubbles from the experimental apparatus, a fully fluidised bed was not thought to be required and, given the large volume of sediment, was not really feasible. A constant stream of water passing through the fixed sediment bed at a speed below the limit of stability, which marks the transition to the fluidised state, was expected to provide sufficient agitation to remove bubbles.

Unfortunately, there is no simple method of determining the quantities of gas bubbles present in saturated sediment and, therefore, no reliable means of gauging the effectiveness of this approach [10]. However, the results presented in later sections prove that the effect of any bubbles that may have been present was insignificant[3].

The layout of the fluidisation system within the laboratory tank is shown in figure 2. A small water pump (44 m head, 40 ℓ / minute peak flow rate) was used to force a stream of water up through the sediment. A nylon mesh filter was fixed over the inlet to prevent sand in suspension from entering the pump, as this certainly would have caused damage. Water was transported in 20 mm diameter plastic conduit and expelled through a series of approximately one hundred 1.5 mm diameter holes. The far end of the conduit was periodically opened (*i.e.*, once every time the system was used) to flush out any sand that had accumulated.

Two consequences of using the degassing system should be noted: Firstly, small particles were lifted into a suspension and remained in the water column for several hours. (The size distribution of particles in suspension was measured, as detailed in

---

[3] A signal-to-noise ratio in excess of 20 dB was achieved after suitable processing was applied to the buried object detection measurements presented in the fourth report in this series. Therefore, it is asserted that any bubbles that may have been present in the sediment did not prevent, or significantly impede, the detection of the buried objects.

section 2.1.2. It was found that most were less than 100 μm in diameter.) The attenuating effects of particles in suspension are considered in section 2.2.3. Secondly, it is known that when fine particles in suspension settle out, they tend to smooth over rough features on the sediment surface [11]. This has the potential to affect the transmission of acoustic energy at the water-sediment interface; a topic that is covered in detail in part 3 of this series[4].

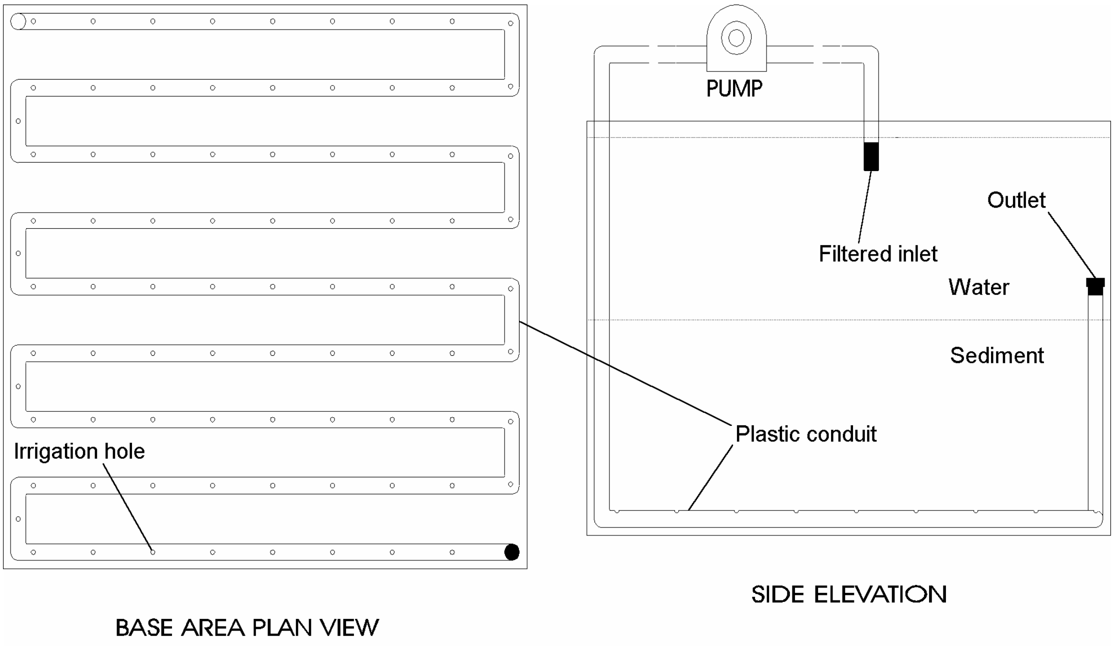

Figure 2 *Schematic layout of the fluidisation system. Bubbles were removed from the sediment by a stream of water, pumped into the conduit and expelled through the irrigation holes.*

One last consideration remains: To prevent out-gassing as a result of the natural breakdown of biological material in the sediment, a small quantity of household bleach was added to the water in the laboratory tank every few months.

[4] R C P Evans and T G Leighton, Studies into the detection of buried objects (particularly optical fibres) in saturated sediment. Part 3: Experimental investigation of acoustic penetration of saturated sediment. *ISVR Technical Report No.* 311 (2007).

2.1.2 Particle Size Distribution

There are several techniques that can be used to determine the size distribution of particles suspended in a fluid, including: particle counting, which is based on measuring the changes in electrical impedance that result from the presence of non-conducting particles suspended in an electrolyte; a settling column, which makes use of the fact that particles of different sizes will settle out from a suspension at different rates; acoustic spectroscopy techniques; and laser light scattering, considered below.

Laser scattering is a flexible sizing technique that can measure the size structure of any material phase provided that it is distinct, optically, from the medium in which it is supported. However, it should be noted that it only provides accurate results for spherical particles. For non-spherical particles, the size distribution is given in terms of an 'effective' spherical particle radius.

Light scattered by particles and the unscattered remainder are incident on a receiver lens. By the process known as 'Fourier optics' [12], the lens performs a two-dimensional Fourier transform of the incident light, forming the far-field diffraction pattern at its focal plane. Wherever a particle is in the light beam, its diffraction pattern will be stationary and centred on the optic axis of the lens.

A detector at the focal plane gathers light over a range of solid angles and gives an output that is proportional to the light energy measured (*i.e.*, the 'radiant flux'). The simplest flux pattern is that from a monomodal dispersion of spheres. It consists of a central bright spot, called the 'Airy disk' [13], surrounded by concentric dark and bright rings, the intensity of which diminish at higher scattering angles. The angle at which the first dark ring occurs depends on the size of the particles, *i.e.*, the smaller the particle, the higher the angle of the first dark ring. By accurately measuring the flux pattern of particles in suspension it is possible to determine the size distribution as the sum of a range of monomodal dispersions.

The sand particle size distribution was ascertained using a laser-scattering-based particle sizer[5]. This comprised an optical measurement unit that formed the basic

---

[5] Access to a Coulter LS Series 100Q laser-scattering-based particle sizer was provided by the University of Southampton, Department of Geography.

particle size sensor, and a computer that managed the measurement and performed results analysis and presentation

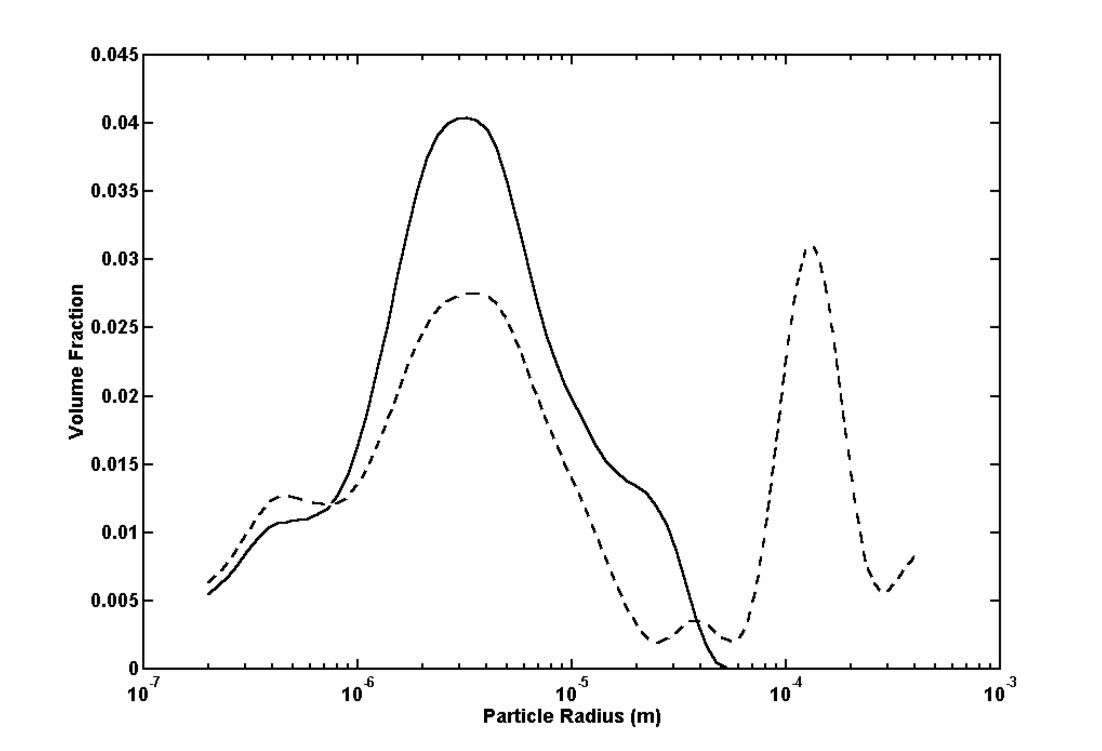

Figure 3 *The measured size distributions of sand particles in a light suspension (solid curve) and from a few centimetres beneath the surface of the sediment in the laboratory tank (dashed curve).*

A suspension was formed by first disturbing the bed to create a cloud of particles and then allowing the larger particles to settle out over a period of a few minutes. (It was observed that it took several hours for the smallest particles in the suspension to completely settle out.) The distribution of particles in the suspension, and from a sample taken from a few centimetres beneath the surface of the bed, are presented in figure 3. From this distribution, the sediment is best described as being a ‘very fine sand’ (using the Wentworth grain size classification [14]).

The two measurements show a similar distribution at small particle sizes, having a peak at a radius of around 3 - 4 μm. The second peak in the bed measurement does not appear in the suspension because the larger, heavier particles settled out quickly whereas the smaller, lighter particles remained in suspension.

2.2 Sound Speed and Attenuation

An acoustic detection system requires sound to propagate through clear water, water containing suspended material, and sediment before interacting with a buried object. The return path also contains such elements. Hence, it was necessary to investigate each component of the acoustic path separately to gain an understanding of the processes affecting the performance of the system as a whole.

In particular, it was necessary to measure the sound speed and attenuation within the water and the sediment in the laboratory tank before undertaking an experimental investigation. In the first instance, this allowed the acoustic behaviour in the test tank to be compared to that found in the ocean. It was also important because:

- **Target location requires accurate sound speed measurements.** An accurate measure of the different speeds of sound within the tank were required. This allowed the positions of scatterers within the sediment to be calculated from the 'time-of-flight' of returned signals. It also made it possible to devise an appropriate position and orientation for the transducer system.

- **Target classification requires accurate attenuation measurements.** Attenuation measurements were necessary for determining optimal frequency ranges for the detection of different classes of target. In order to do this, of course, the scattering characteristic of the target must be known, as well as the system transfer function and the background noise spectrum. Such classification issues will be discussed in the fourth report in this series[6], which deals with the practical detection of buried objects.

2.2.1 Sound Speed

The speed of sound in a liquid, c_f, depends on its equilibrium density, ρ_f, and bulk modulus, K_b, according to the relationship, $c_f = \sqrt{K_b/\rho_f}$. In seawater, this is a function of temperature, pressure and salinity [15]. There are a number of empirically-

---

[6] R C P Evans and T G Leighton, Studies into the detection of buried objects (particularly optical fibres) in saturated sediment. Part 4: Experimental investigations into the acoustic detection of objects buried in saturated sediment. *ISVR Technical Report No.* 312 (2007).

derived formulae that can be used to predict the speed of sound in seawater (*e.g.*, the Leroy equations [16, 17]). In addition, the sound speed in the ocean depends on a range of phenomena such as the surface bubble layer [18].

The sound speed profile observed in the deep ocean is, typically, similar to that shown in figure 4. Within the first few metres of the ocean surface, it can be dominated by the presence of bubbles. At greater depths it decreases with temperature, exhibiting seasonal variations over the first 100 m. At mid-latitudes, the minimum sound speed occurs at depths of below around 1 000 m (although it can occur at much shallower depths at the poles). Below this region, the water temperature remains nearly constant and sound speed increases linearly with pressure [19].

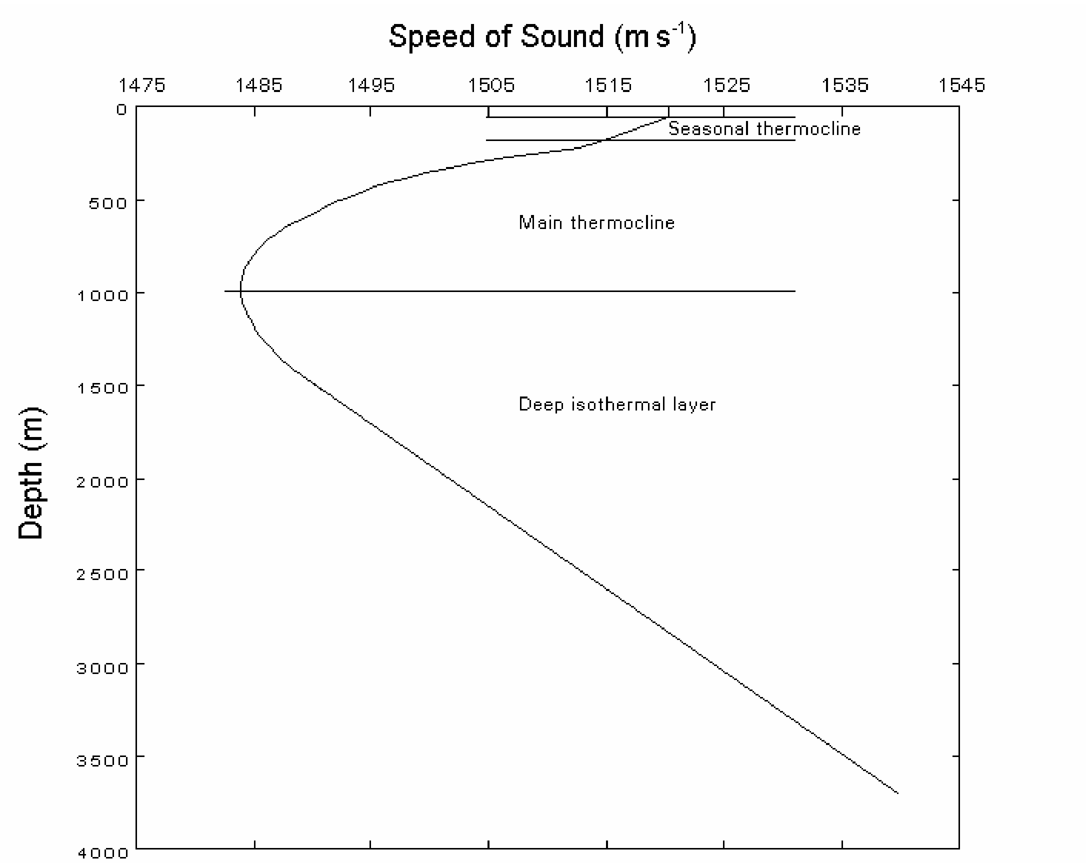

Figure 4 *The typical sound speed profile observed in the deep ocean*[7] *[20].*

[7] For clarity, a constant sound speed profile has been shown in the top 50 metres of figure 4. This region is known as the surface, or mixed, layer and it is subject to considerable variation. However, for the purpose of the laboratory investigation, it is not relevant since the region of interest is at a depth of around 1 kilometre.

The speed of sound in sediments can be predicted using various models. It should be noted that several types of wave can propagate through sediments, *i.e.*, compressional, shear and interface waves [21]. However, for the purpose of this investigation, only the normal compressional wave (or 'p-wave') is considered in any detail. (The existence and consequences of the other waves are considered in the next report in this series[4].) The speed of sound in sediment is dependent on the bulk moduli of the fluid, the solid grains and the frame [22]. It is generally accepted that phase dispersion in both seawater and in sediments is negligible over any practical frequency range.

The sound speeds in the water and the sediment were measured using a simple arrangement of two hydrophones[8] separated by a distance of 1 m ± 1 cm, as shown in figure 5. In the first arrangement the hydrophones were independently suspended in the middle of the water column. Hydrophone, Tx, was used as a source and was excited using a single-cycle sine wave pulse, having a centre frequency of 75 kHz[9]. The transmitted acoustic pulse was received by the second hydrophone, Rx. In the second arrangement, the hydrophones were positioned 20 cm below the water-sediment interface. A similar acoustic pulse was generated by Tx and received by Rx. The time delay between the output and the returned pulse was measured in both cases.

---

[8] Brüel & Kjær type 8103 hydrophones were used in the experiments described in this report and in the experiments described in the reports referenced in footnotes 4 and 6. Although being termed 'hydrophones', which are transducers that convert sound into electricity [23], piezoceramic transducers of this type can also be used as acoustic sources.

[9] The spectrum associated with a single-cycle sine wave pulse, centred on 75 kHz, is continuous and broadband. The 3 dB bandwidth of such a pulse extends from 31.1 kHz to 98.0 kHz. If the response of the hydrophone (which was found to have a peak at around 120 kHz when used as an acoustic source) is also taken into consideration, then most of the transmitted acoustic energy is found to lie between 75 kHz and 100 kHz.

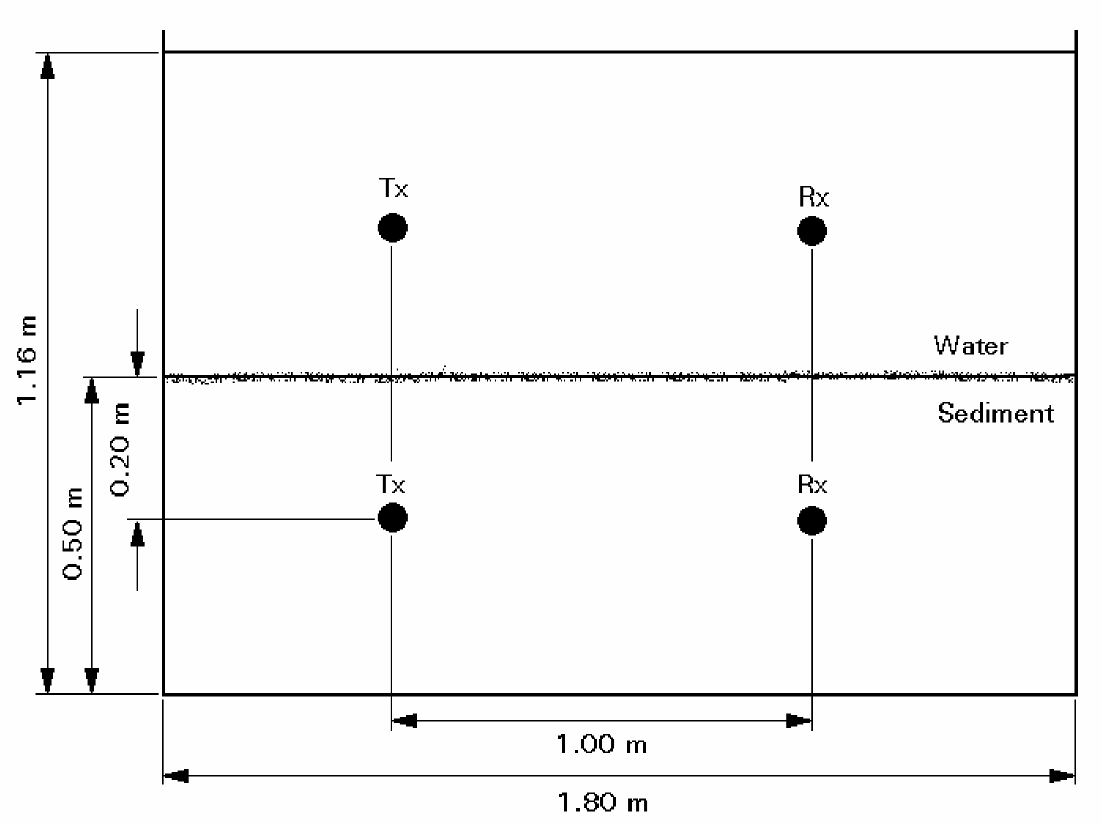

Figure 5 *Side view of the source / receiver arrangement for the speed of sound measurements in water and water-saturated sediment in the laboratory tank.*

The sound speeds were calculated from the travel times of the acoustic pulses. They were found to be 1 478 m s^{-1} in water and 1 692 m s^{-1} in the sediment, with an error of ± 2 % in each case. (This error was based on the tolerance in the misalignment of the hydrophones.) The water temperature, T, was measured to be 16.5 °C ± 0.5 °C and the atmospheric pressure, P_{atm}, was measured to be 1 006 mbar ± 0.5 mbar.

The speed of sound in distilled water can be found from the empirical formula [24]:

$$c_f = 1402.7 + 488t_g - 488t_g^2 + 135t_g^3 + \left(15.9 + 2.8t_g + 2.4t_g^2\right)\left(\frac{P_g}{100}\right) \qquad (1)$$

where $P_g = P_{atm} / 1000$ is the gauge pressure and $t_g = T / 100$. This equation should be accurate to 0.05 % in the range $0 \le T \le 100$ °C and $0 \le P_g \le 200$ bar. Hence, from the measured values of temperature and pressure, the speed of sound was predicted to be around 1 471 m s^{-1} (in fact, 1 470.7 m s^{-1} ± 0.17 m s^{-1}).

The calculated result for distilled water agrees with the measured result for the tank water to within the estimated error[10]. From a comparison of the measured sound speed with that shown in figure 4, it can be seen that the speed of sound in the tank was similar to that found in the deep ocean.

The agreement shown between the measured and theoretical values in water suggests that the measured value for the speed of sound in the sediment should be reasonably accurate. Unfortunately, a comparison with the measured values available in the literature is difficult since real sediments display a wide range of sound speeds (from 1500 - 1900 m s^{-1}) depending on their composition and geographical location [25]. However, the same literature also indicates that sound speed increases with mean grain size. It is interesting to note that the sound speed measured in the laboratory tank corresponds to grain diameters of less than 100 μm, which compares favourably with the particle size distribution measured in section 2.1.2.

(Attenuation in the sediment was also of particular interest. There are relatively few measurements available in the literature for sandy sediments over the range of frequencies used in this investigation. Therefore, the attenuation in the sediment in the laboratory tank was measured, as described in section 2.2.4.)

2.2.2 The Attenuation of Sound in Seawater

The attenuation of sound in seawater in the range 1 kHz - 1 MHz is attributed to three main absorption processes. The effects of shear viscosity [26] and volume viscosity [27] account for the absorption observed in distilled water, and in seawater the dominant cause of absorption at frequencies below 100 kHz is ionic relaxation. This is a chemical disassociation / reassociation process which occurs over a finite relaxation time [28].

Both the ionic relaxation mechanism and viscous absorption are dependent on frequency, salinity, temperature and pressure. An empirical equation based on laboratory data was presented by Fisher and Simmons [29, 31]. This result,

[10] One would not be surprised if a more precise measurement showed that the speed of sound in distilled water was slightly lower than the result for the water in the tank, since tap water contains impurities.

summarised in figure 6, includes the contributions from the two ionic compounds in seawater that have the strongest relaxation effect: magnesium sulphate and boric acid.

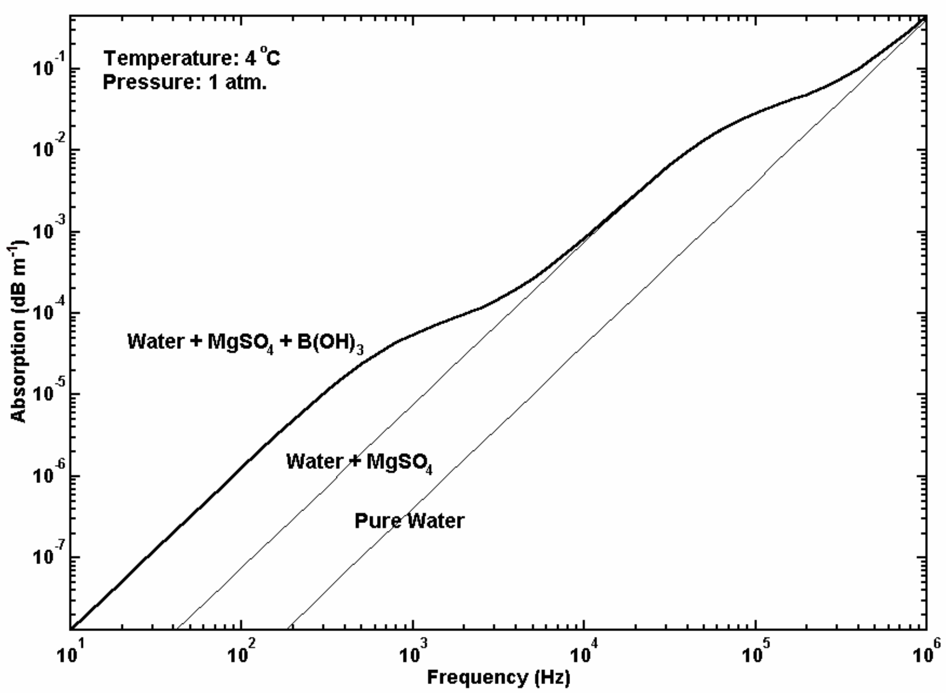

Figure 6 *The absorption coefficient in seawater according to the expression of Fisher and Simmons [29] in Lyman and Fleming seawater [30] of salinity 3.5 % and pH = 8.0. The thick solid line is the combined absorption for pure water and the ionic compounds, magnesium sulphate and boric acid.*

2.2.3 The Attenuation of Sound in Suspensions

Small quantities of suspended material can have a significant effect on the attenuation of sound waves. In suspensions, attenuation is attributed to three main loss mechanisms: scattering by particles [3]; viscothermal absorption [32]; and the intrinsic absorption of acoustic energy by the water itself.

Scattering can be characterised in terms of the ‘form function’, which is proportional to the ratio of the re-radiated pressure to the incident pressure as a function of angle and distance from the scattering centre. When evaluated for monostatic scattering, it is proportional to the acoustic back-scatter cross-section [33, 34]. In general, theoretical models for the form function treat particles in suspension as a cloud of homogeneous spheres [3] which exhibit characteristic resonances in response to an acoustic signal [35]. Conversely, naturally occurring sediments are irregular and inhomogeneous with the consequence that well-defined resonances do not occur.

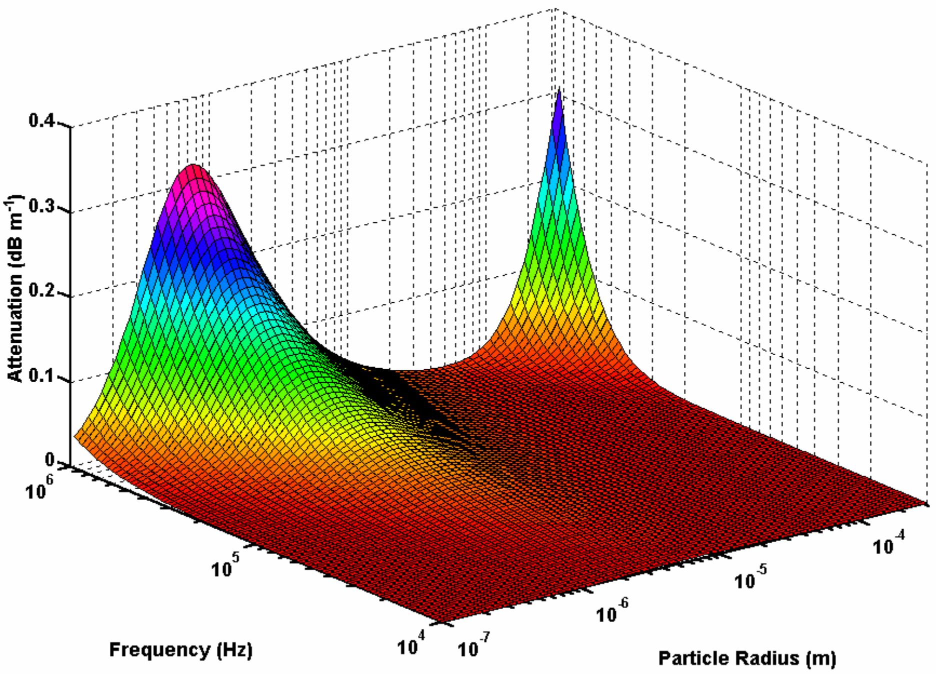

Figure 7 *The attenuation coefficient due to scattering and absorption as a function of acoustic frequency and particle radius for a suspension of spherical quartz particles with a mass concentration of 0.2 kg m*$^{-3}$ *[36]. (Original in colour.)*

Richards and co-workers [36] have taken a different approach to the scattering mechanism, using a heuristic model based on a modified form of the 'high-pass model' [37] as employed by Sheng and Hay [38]. This model also includes viscothermal losses, whereby sound energy is converted to heat by friction in the viscous fluid boundary around particles in suspension [32], and the absorption effects detailed in section 2.2.2.

Figure 7 shows the theoretical attenuation coefficient associated with a suspension of spherical quartz particles in seawater, as calculated by Richards [36]. The peak at small particle sizes is due to viscothermal absorption. The second peak is due to scattering and becomes more significant for larger particles at higher frequencies.

Recent experimental work using suspensions of spherical[11] quartz particles has shown good agreement with the theoretical predictions for the attenuation coefficient [41].

The size distribution of a suspension of sand particles in the laboratory tank has been measured, as detailed in section 2.1.1. The distribution exhibits a peak at a radius of around 3 - 4 μm, which is close to the theoretical viscothermal absorption peak shown in figure 7. Also, the accompanying size distribution for particles in the sediment bed shows that a sizeable fraction of the sediment is composed of particles that are not far removed from the scattering peak shown in figure 7. These observations imply that the attenuation coefficient associated with a suspension of sediment in the laboratory tank should be high.

In order to estimate the attenuation coefficient for a real particle size distribution, the attenuation spectrum for each size bin must be calculated individually. The weighted sum of these spectra gives the total attenuation spectrum, where the weighting for each size bin is equal to the product of bin height and width. This calculation was performed for the measured distribution of sand grains in suspension with an arbitrarily chosen mass concentration of 0.2 kg m^{-3}, as shown in figure 8.

The concentration of suspended material used in this calculation is unusually high for deep water regions, being more typical of the concentrations found in coastal and estuarine waters [36]. The total attenuation would be significant for high frequency sonar systems which operate in such regions over path lengths of up to several hundred metres [42]. However, for the purpose of this investigation, where the total path length and the concentration of suspended material are considerably less, the total attenuation was considered negligible.

[11] It should be noted that Richards' theory was originally developed for suspensions of spherical particles (or near-spherical particles which, on aggregate, may *scatter* sound in a similar manner to a suspension of spherical particles [39]). However, some naturally occurring sediment materials are distinctly non-spherical, *e.g.*, clay particles are plate-like in appearance, having aspect ratios of around 30:1. Recent experimental work on the absorption associated with such particles has shown limited agreement with the theory, in which the particles are assumed to be viscous fluid spheres suspended in a viscous fluid [40].

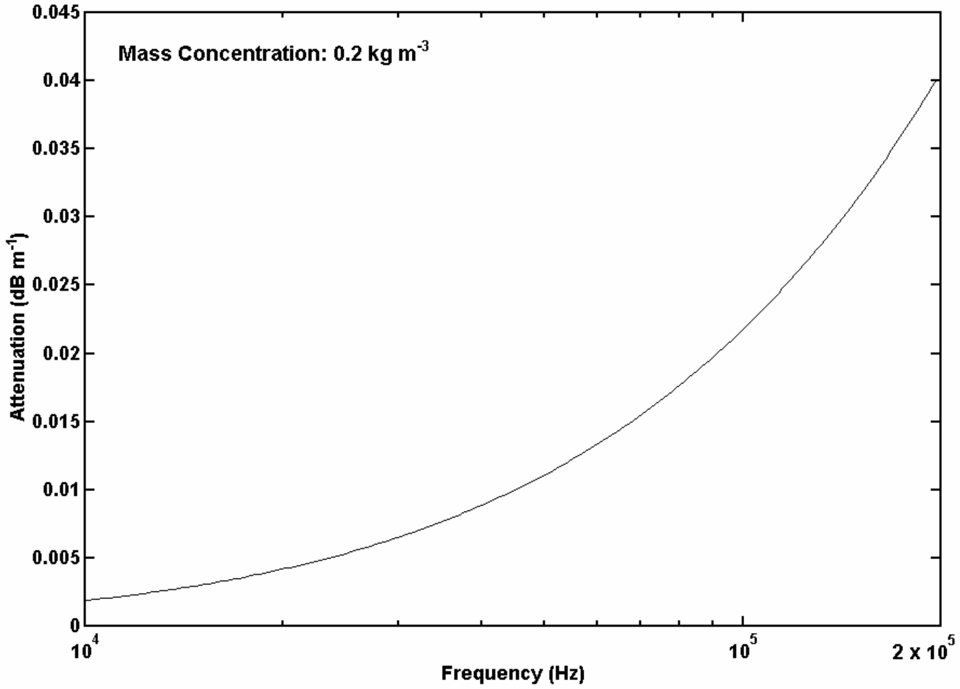

Figure 8 *The attenuation coefficient calculated for a suspension of sand particles in the laboratory tank with a mass concentration of 0.2 kg* m^{-3}.

2.2.4 The Attenuation of Sound in the Seabed

It is generally accepted that sound energy is absorbed in the seabed by a combination of frictional losses at inter-particle contacts, and by viscous losses caused by the movement of the pore fluid relative to the solid frame [43]. However, the precise details of the attenuation mechanism are subject to debate. (It is noted in section 2.2.1 that several types of wave can propagate in sediments in addition to the primary compressional wave. These are considered in detail in the next report in this series[4].)

A considerable body of attenuation data is available in the literature for a range of sediment types at numerous geographical locations. On the basis of this evidence it has been argued by researchers such as Hamilton [2] that the attenuation coefficient, α_{dB}, of plane compressional waves in marine sediments varies with frequency, f_k, according to the relationship

$$\alpha_{dB} = k_\alpha f_k^{\,n_\alpha} \tag{5}$$

where α_{dB} is measured in dB m^{-1}, f_k is expressed in kHz and k_α and n_α are constants. A summary of the data relevant to this investigation is shown in figure 9.

Attenuation appears to scale linearly with the first power of frequency (*i.e.*, $n_\alpha = 1$) over the range of measurements shown in figure 9. It is useful to approximate the attenuation coefficient by using a value of $k_\alpha = 0.5$ (shown on the graph as a solid line). This approximation is reasonably accurate for the available sand data and a good estimate for the data pertaining to sand, silt and clay. However, there are still relatively few measurements for sandy sediments between 10 kHz and 100 kHz (the frequency range that is of particular interest in this investigation).

The attenuation coefficient for the sediment in the laboratory tank was measured using a broadband pulse technique and a simple attenuation model. An 'in-situ' technique was preferred over the more conventional method of measuring attenuation with an impedance tube [44]. This was because it was desirable to minimise the disturbance to the sediment in the laboratory tank. Also, it was difficult to ensure that sediment taken from the tank did not contain any air or excess water, or that the size distribution did not change as a result of small particles being swept up into the water column.

The preferred method would have been to generate a single-frequency, continuous-wave (CW) acoustic signal from a source buried in the sediment, and to have measured the sound pressure at various distances from the centre of the source. Repeating the measurement for a range of different frequencies would have allowed the attenuation spectrum to have been determined with a high degree of accuracy. Unfortunately, CW signals could not be used effectively in the laboratory tank because of its relatively small size. Reflections from the tank walls, *etc.*, would have interfered with the signal at the receiver within too short a time frame to have allowed useful measurements to be obtained.

An alternative to CW signals would have been to use short, broadband pulses. However, pulses of this type are somewhat limited in power and are easily distorted, resulting in the output power spectrum being poorly defined. A better alternative was found in the linear-swept, frequency-modulated (or 'chirp') pulse. This type of signal is broadband but can be stretched out in time, which reduces transient distortion and allows more energy to be transmitted [46]. (Chirp pulses have a number of useful properties which make them of particular interest in this investigation. Their use in an acoustic detection system is considered further in a subsequent report in this series[6].)

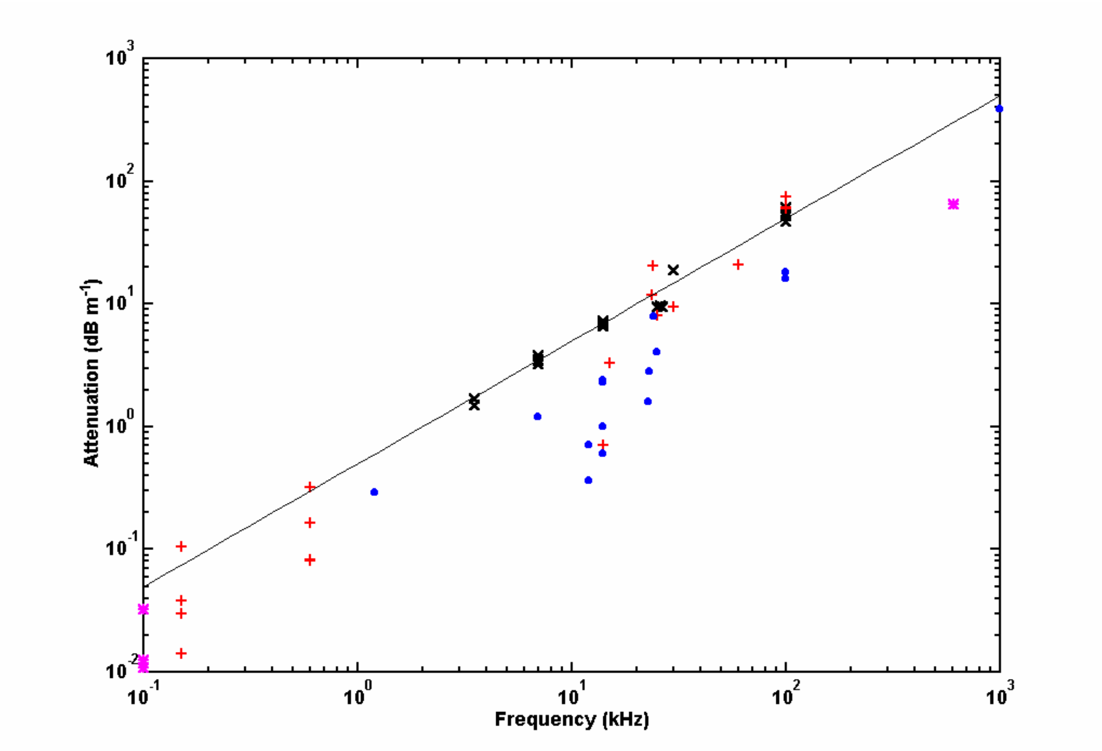

Figure 9 *The attenuation coefficient measured in a range of naturally occurring, saturated marine sediments [2, 25, 45]. Symbols:* × *= sands, all grades;* + *= sand-silt, silt-sand, sand-silt-clay;* ● *= clay-silt, silt, silt-clay; and* ♦ *= various clays. The straight line corresponds to an attenuation coefficient of* $\alpha_{dB} = 0.5 f_k^{\ 1}$. *(Original in colour.)*

In practice, a 1 ms long chirp pulse, sweeping upwards in frequency from 20 kHz to 150 kHz, was used to drive the acoustic source. A $^{1}/_{10}$ cosine-tapered window was applied to minimise transient distortion, resulting in the useful frequency range of the pulse being reduced to 33 - 137 kHz. The duration of the pulse was chosen to be as long as possible before reflections within the tank would have become a problem.

The arrangement of the acoustic source, Tx, and receiver, Rx, are shown in figure 10. Hydrophones were used as both source and receiver elements. The first hydrophone, Tx, was positioned 25 cm below the water-sediment interface and near to one end of the tank. The second hydrophone, Rx, was positioned at a similar depth and near to the opposite end of the tank. For each set of measurements the position of Tx was kept fixed and Rx was moved progressively closer. The distance between the two hydrophones, x, was noted in each case with an estimated accuracy of ± 1 cm.

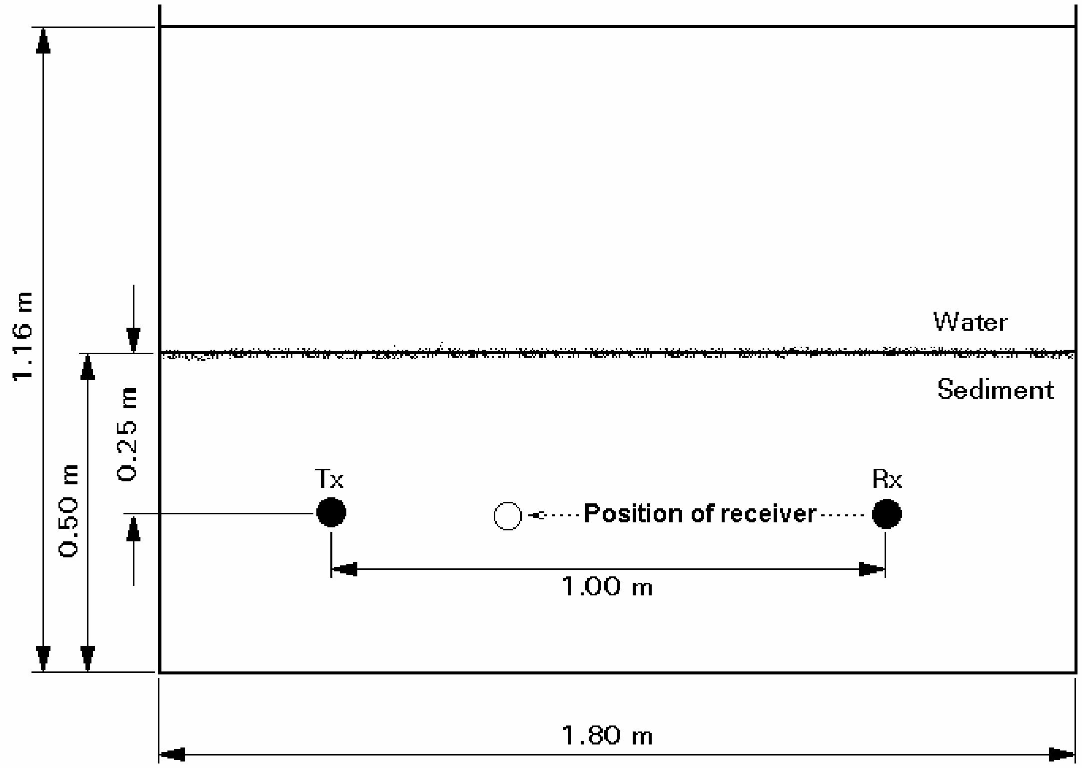

Figure 10 *Side view of the source / receiver arrangement for the sediment attenuation measurement in the laboratory tank. The filled symbols represent the initial positions of the acoustic source, Tx, and receiver, Rx. The outlined symbol represents the range of positions of the receiver.*

In order to interpret the signals recorded at the receiver, it was necessary to formulate a simple attenuation model. It was assumed that all measurements were performed in the far-field of the transducers and that they exhibited an omni-directional response[12]. Thus, a simple geometrical spreading function was used, with pressure amplitude varying as the inverse of distance. By assuming that the contribution due to noise was

[12] According to the manufacturer's data, the variation in hydrophone sensitivity should have been less than 3 dB in every direction at a frequency of 100 kHz [47]. Furthermore, the data suggests that the sensitivity variation would been less than this at frequencies below 100 kHz.

negligible, a frequency-domain representation of the recorded signal, S(ω), can be written:

$$\left|S(\omega)\right| = \left|\Psi(\omega)H(\omega)\right| \tag{6}$$

where Ψ(ω) is the driving signal and H(ω) is the transfer function of the complete physical system. Both S(ω) and H(ω) are functions of frequency and of the separation between the source and receiver, x.

The transfer function can be separated into its separate components,

$$H(\omega) = \exp\left[-a_{np}(\omega)x\right]X(\omega)\frac{1}{x^{\Delta}} \tag{7}$$

where X(ω) is the response of the detection system (including the signal generator, charge amplifier, power amplifier, *etc*.), a_{np} is the attenuation coefficient in np m^{-1} (where $\alpha_{dB} = (20\log_{10} e) \times a_{np}$ dB m^{-1}), and Δ is the directivity function. Substituting this expression into equation (6) and taking the natural logarithm allows the individual terms to be separated:

$$\ln|S| = \left(\ln|\Psi| + \ln|X|\right) - a_{np}x - \Delta \ln x \tag{8}$$

The directivity function, Δ, is equal to unity in the far-field. Given the separation, x, this equation can be expressed in terms of just two parameters: $\left(\ln|\Psi| + \ln|X|\right)$ which is a constant; and the attenuation coefficient, a_{np}.

By taking measurements at two positions, x_1 and x_2, and subtracting, the constant parameter disappears to leave

$$\ln|S|_{x=x_2} - \ln|S|_{x=x_1} = \Delta\left(\ln x_1 - \ln x_2\right) - a_{np}\left(x_1 - x_2\right) \tag{9}$$

which only has one unknown, a_{np}.

From this analysis it would seem that only two measurements are required to determine the attenuation coefficient. However, each measurement is subject to noise, to variations in attenuation over the specific propagation path, and to positional error in the transducers. A much better estimate of the attenuation coefficient is obtained by taking measurements at $\left(\ln|\Psi| + \ln|X|\right)$ different positions, giving n equations in the form of equation (9). The average of n estimates of the attenuation coefficient gives a much more accurate value[13].

In total five sets of data were recorded over two days, separated by a period of several weeks. The water temperature and the atmospheric pressure were recorded as being 15.5 °C ± 0.5 °C and 1014 mbar ± 0.5 mbar on the first day, and 16.2 °C ± 0.5 °C and 1016 mbar ± 0.5 mbar on the second day. Each set of data comprised 21 measurements spaced 2.5 cm apart, with every measurement being the average of 100 recorded pulses. Thus, the five sets of data each provided 20 estimates of the attenuation coefficient; 100 estimates in total. The averaged results are presented in figure 11, alongside the historical data for attenuation measured in sands. The straight line on the graph corresponds to the approximation, $\alpha_{dB} = 0.5f_k^{\ 1}$.

The attenuation measured in the laboratory tank was slightly less than that measured in the naturally occurring sands though it closely follows the empirical law, scaling linearly with the first power of frequency. A best-fit line, following the linear scaling law, was fitted to the laboratory data using a regression algorithm. The value of k_α was found to be 0.41 with a standard error on the regression estimate of 2.5 dB m^{-1}.

It should be noted that the acoustic insertion loss [48] experienced by hydrophones when they are used in sediment differs from that when they are used in water. In order to determine this difference, a similar set of measurements was obtained in water and a best-fit line was fitted to this new data. By comparing the standard errors on the regression estimates for the in-water and in-sediment measurements, an estimate of the insertion loss associated with hydrophone measurements in water-saturated sand was obtained. The sensitivity of the hydrophone in sand was found to vary by around ± 1 dB from its in-water sensitivity.

---

[13] Since the measurements were performed over different days, they were compared to ensure that there was no consistent variation between them as a result of any changes in the measurement conditions. Such a variation was not found to occur. The average and the standard deviation of the attenuation coefficient was calculated as follows: Firstly, the logarithmic values were converted into a linear system of units. The averages and the standard deviations were then calculated. Finally, the linear results were converted back into the logarithmic system of units.

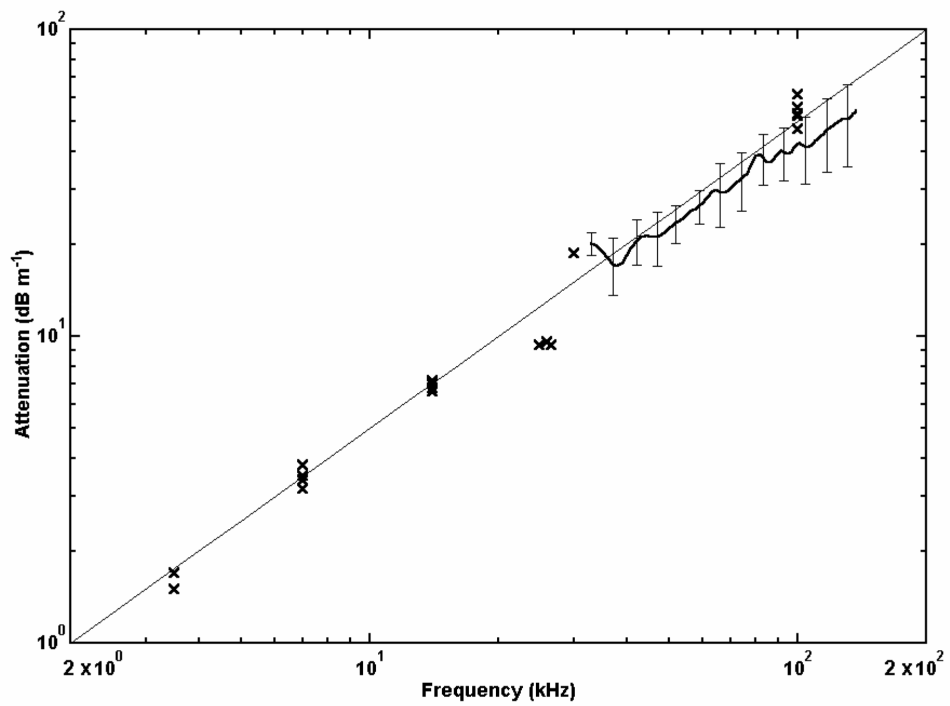

Figure 11 *The average attenuation coefficient measured in the laboratory sand is marked by the curve. The error bars at selected frequencies correspond to a standard deviation of ±1. A subset of the historical data (see figure 9) for a range of sandy sediments are marked by the points, ×. The straight line corresponds to an attenuation coefficient of* $\alpha_{dB} = 0.5 f_k^{\ 1}$.

The attenuation of sound in the sediment is the most important attenuation process thus far considered, having a significantly greater effect than the attenuation processes in water and suspensions of particulate material. A comparison of the different sources of attenuation and the implications for an acoustic detection system are presented in section 2.3.

2.2.5 The Seawater-Seabed Interface

The behaviour of acoustic waves in naturally occurring, inhomogeneous sediments is complicated, since acoustic wave energy can be divided between shear and interface waves as well as reflected and transmitted compressional waves [22, 49]. Surface roughness can also have a significant effect on the transmission of acoustic waves, especially at shallow grazing angles. The propagation of acoustic waves in sediments, with particular consideration given to roughness scattering at the interface, is dealt with in the next report in this series[4].

In the initial stages of the investigation it was assumed that the sediment could be modelled as a simple, homogeneous fluid with a plane interface. In this case, energy is divided between reflected and refracted compressional waves with the angle of transmission depending on the angle of incidence and the acoustic properties of the fluid media [50]. It has been noted by other authors that useful results can still be obtained with this approach [51].

Consider a scalar wave, ψ_i, incident on the boundary with reflected and transmitted waves ψ_r and ψ_t respectively. The required boundary conditions are that the tangential field (along the interface in the *x*-direction), ψ_x, is continuous and that $\psi_i + \psi_r = \psi_t$. No assumptions are made about the directions of the reflected and transmitted waves. It can be shown that the angle of reflection is equal to the angle of incidence and that the angle of transmission of the refracted wave is governed by Snell's law [52]:

$$\frac{\sin\theta_i}{c_1} = \frac{\sin\theta_t}{c_2} \tag{10}$$

where θ_i and θ_t are, respectively, the angles of incidence and transmission of waves going from the first medium, with a sound speed, c_1, into the second medium, with a sound speed, c_2.

At a critical angle of incidence, θ_c, the angle of transmission reaches 90°. It is evident that for $\theta_i \geq \theta_c$ no energy is transmitted into the second medium and the incident wave is said to undergo 'total internal reflection' [53]. However, if there is no transmitted wave the boundary condition ($\psi_i + \psi_r = \psi_t$) cannot be satisfied. Therefore, it is asserted that a transmitted wave does exist but that it cannot, on average, carry energy across the boundary. This leads to a transmitted field vector of the form,

$$\Psi_t = A\exp(\mp Bz)\exp\left[j\left(\omega t - k_i x \sin\theta_i\right)\right] \tag{11}$$

where k_i is the wave vector of the incident wave. The factor exp(+Bz) defines an exponential growth of ψ_t as a function of penetration depth, z, which is physically untenable. The alternative is a wave which decays exponentially in amplitude as it penetrates the second medium. This disturbance travels along the interface in the x direction and is known as an ‘evanescent wave’ [53].

If the ‘fluid-fluid’ interface is assumed to be massless, the pressure amplitude transmission, T_{Pa}, and reflection, R_{Pa}, coefficients can be found from the conservation of particle velocity and the continuity of pressure at the boundary [52]:

$$R_{Pa} = \frac{Z_2/Z_1 - \cos\theta_t/\cos\theta_i}{Z_2/Z_1 + \cos\theta_t/\cos\theta_i} \quad \text{and} \quad T_{Pa} = 1 + R_{Pa} \tag{12}$$

where Z_1 and Z_2 are the characteristic acoustic impedances of the media (the product of volume density and the thermodynamic speed of sound). For sediments of low porosity, *e.g.*, red clay, calcareous ooze, silt and fine quartz sand, the assumption of a simple reflection loss is often valid [54].

The power transmission, T_π, and reflection, R_π, coefficients are simply related to the pressure amplitude coefficients by $R_\pi = |R_{Pa}|^2$ and $T_\pi = 1 - R_\pi$. For the sediment in the laboratory tank, R_π was calculated to be less than 0.3 for angles of incidence up to, approximately, 50°.

2.3 Summary of design considerations for sediment tank

In sections 2.1 and 2.2, above, the acoustic test facility and the physical nature of the acoustic media have been described. The sediment was principally composed of sand particles which were, to a first approximation, spherical and similar in size to sand particles found in the deep ocean. Their size distribution was measured using an optical technique and was found to be bimodal with peaks at effective spherical radii of a few microns and around 100 μm.

Sound speed and attenuation were identified as being important parameters in the design of a detection system. A straightforward technique was used to determine the speed of normal compressional waves in water and sediment. In water, the measurement was found to be in good agreement with an empirical sound speed model. Having validated the measurement technique in water, the sound speed measurement in sediment was assumed to be reasonably accurate. (Unfortunately, historical data for similar sediment types cover a wide range of sound speeds. Hence, no direct comparison could be made.)

Attenuation has been estimated for each component of the propagation path, *i.e.*, the water, suspensions, and the sediment. The attenuation of sound in water is covered, extensively, in the literature. In seawater, the attenuation coefficient is, typically, around 10^{-2} dB m^{-1} in the 10 - 100 kHz range [29]. In pure water, it is an order of magnitude lower.

The attenuation of sound in suspensions is a relatively new topic of research. In the literature, theoretical models show good agreement with practical measurements for spherical particles, and limited agreement for non-spherical particles [41]. The attenuation associated with a suspension of sand in the laboratory tank was calculated using the particle size distribution data, noted above. Even for an artificially high concentration of suspended material (0.2 kg m^{-3}), the attenuation coefficient was still found to be negligibly small (less than 5×10^{-2} dB m^{-1}) in the 10 - 100 kHz range.

The attenuation of normal compressional waves in the sediment has also been considered. A set of measurements were performed in the laboratory tank, and a value for the attenuation coefficient was calculated using a simple attenuation model. It was found to scale linearly with frequency, although the value obtained for the laboratory sand was slightly lower than in naturally occurring sands (by 0.09 dB m^{-1} kHz^{-1}). It should also be noted that sands are, generally, more highly attenuating than other sediment types such as silts and clays.

The interaction of sound at the seawater-seabed interface has also been considered, albeit very briefly. This is a complex area of study that is of particular interest in this investigation. Therefore, it is revisited in considerably more detail in the next report in this series[4]. For the purpose of assessing the feasibility of an acoustic detection system, however, it was noted that the seabed can be modelled as a simple, homogeneous fluid with a plane interface. For completeness, the pressure amplitude transmission and reflection coefficients for a fluid-fluid interface were also noted.

The attenuation processes in seawater are relevant to many areas of study in underwater acoustics [19]. However, the most significant loss mechanism in the present investigation is the attenuation of sound in the sediment. In the 10 - 100 kHz range, the attenuation coefficient in water-saturated sand varies from 5 - 50 dB m^{-1} (compared with attenuations of less than 0.1 dB m^{-1} in water and suspensions).

The implication for a detection system is quite obvious. The sound pressure developed by the source must be high enough that acoustic waves can penetrate the sediment, and usefully interact with a target buried at a depth of up to 1 m. However, an increase in the acoustic power of the source is necessarily accompanied by an increase in the reverberation level in the medium, *i.e.*, the scattering of the emitted signal from the seabed surface and volume inhomogeneities within the sediment [33].

Hence, the receiver must be designed to have a narrow beamwidth, in order to prevent reverberant energy from dominating the incoming acoustic signal. The design of the transducer system is presented in section 3. In addition, signal processing techniques can be used to extract useful target information from high levels of background noise and clutter. Several approaches, ranging from simple time windowing to more advanced techniques, such as optimal filtering, are presented in a later report in this series[6].

3 Transducer Design

A source and receiver can be arranged either monostatically or bistatically, *i.e.*, the source and receiver can be combined in a single unit or they can be located separately. Ordinarily, a monostatic arrangement would be the preferred choice for an ROV-mounted system. (ROVs are generally built to house modular, compact devices, and a single unit would offer advantages in terms of ruggedness, ease of alignment, simplicity of installation, *etc*.) However, in the laboratory it was considered better to use separate units that would be easier to install and operate.

It was important that as much of the energy radiated from the source as possible was directed towards the suspected position of buried objects in order to maximise the interaction within the target volume. Therefore, a high acoustic source power and a narrow beamwidth were specified. Similarly, the receiver was required to be directed towards buried objects to reduce background noise, thus improving the overall signal-to-noise ratio.

Many commercial sonar systems exhibit such characteristics [55]. Notable amongst these are parametric sonar systems [56] that exploit the non-linear property of water, *i.e.*, a change in density caused by a change in pressure of a sound wave in water is not linearly proportional to the change in pressure. In any such non-linear system, the frequencies produced at the output are different to those at the input. These secondary frequencies, which may include harmonic and sub-harmonic frequencies, only occur at 'high' amplitudes of the primary wave. With a parametric sonar there is no sidelobe radiation outside of the main beam; the beamwidth is narrow and nearly constant over a broad range of frequencies; the sonar exhibits an inherently broad bandwidth; and projector cavitation does not pose a problem. However, systems such as these were considered to be too expensive to be used in this study. Therefore, a directional transducer system was purpose-built for use in the laboratory. Fortunately, there was considerable scope in the design of the transducers to enable a high power and narrow beamwidth to be achieved. Two techniques were considered in some detail:

- **Beamforming.** The interference pattern that results from the linear superposition of an array of monopole sources radiating at the same frequency can have a pronounced directivity [57]. This can be controlled by changing the relative phase of the sources. For the purpose of this investigation, an 'ideal' beam pattern would comprise a narrow central lobe with minimal sidelobes. However, in a highly directional array a significant proportion of the source power can leak away to the sidelobes. This can be reduced by applying a windowing function to the array, but only at the expense of directionality.

  It should be noted that classic array signal processing techniques assume that plane waves are reformed at the array, *i.e.*, operations are performed in the acoustic far-field. Array techniques become sub-optimal close to the array. Furthermore, the range of frequencies that can be generated before spatial-aliasing occurs is limited by the separation of the sources [58].

- **Acoustic reflector.** A curved acoustic reflector can be used to focus the power radiated from an omni-directional source into a narrow beam [59]. However, the direction of the beam cannot be steered electronically, as is the case for the beamforming array, but instead requires the source / reflector assembly to be repositioned. The focal length can be varied by changing the position of the source relative to the back of the reflector. However, the relationship between the source position and the focus is logarithmic which can make it difficult to set the focal length accurately.

The acoustic reflector and the beamforming array are both established techniques for producing a tightly confined acoustic beam. The array has the advantage of being able to produce a higher output power than the reflector because more than one source element is involved. However, on the grounds of its relative simplicity and cost-effectiveness, the acoustic reflector approach was adopted for this application.

Some alternative techniques have also been considered. For example, iterative, time-reversal focusing could provide a means of developing a high acoustic power in the region of the target [60, 61, 62]: An array of transmit and receive transducers can be used to insonify a target volume and record the back-scattered signals. If these signals are time-reversed and re-emitted, the transmitted signal should refocus on any reflective scatterer within the target volume. If the medium is largely homogeneous, but contains several scatterers, the time reversal process can be made to focus on the most reflective one by iteration. The array can also be curved, like the acoustic reflector, to become both electronically and geometrically focused [63].

This approach would seem to combine the best of both transducer designs (*i.e.*, high power, narrow beamwidth, and electronically adjustable focusing) and would be a natural extension of the acoustic reflector arrangement for use in the field. However, there are two major drawbacks associated with this method: it becomes ineffective if the attenuation in the surrounding medium is high; and substantial computing power is required.

3.1 The Design of an Acoustic Reflector

Acoustic reflectors are somewhat analogous to optical mirrors and to reflectors of the sort that are frequently used in the field of radar. A paraboloidal mirror will, upon reflection, reform an incident plane wave into a converging spherical wave. Similarly, an ellipsoid and hyperboloid will both produce perfect imagery between pairs of conjugate axial points corresponding to their two foci [64]. (In practice, the ellipsoid must be mounted at a greater distance from the source than the hyperboloid.) A spherical mirror, which constitutes a special case of the ellipsoid, is virtually identical to a parabola in the paraxial focusing region and, in general, will suffer less aberration than its aspheric counterparts. Spherical mirrors are also much easier to fabricate than aspheric surfaces, especially in the case of large reflectors. This is an important consideration since surface features must be controlled to within much less than the wavelength of the incident radiation to keep diffraction to a minimum.

In order to collect as much of the source power as possible, a large reflector aperture was required. Buckingham used a 3 m diameter, spherical reflector in his acoustic daylight™ experiments [59, 65]. This comprised a pressure-release surface made from neoprene rubber bonded to a fibreglass shell. Potter later demonstrated that a smaller dish would have resulted in a better confinement of the acoustic beam [66]. In this investigation, the maximum reflector size was constrained by the dimensions of the laboratory tank and, to some extent, by the cost of fabrication. Therefore, a simple comparison between a range of reflectors having different diameters was performed using a ray tracing algorithm.

A description of the reflector geometry and the details of the algorithm used to determine its focusing characteristics are presented in appendix A. The caustic curve bounding the acoustic field was found by the application of Fermat's principle [67]. This states that the actual ray path between two points is the one that is traversed in the least time. A useful figure of merit for the caustic is the diameter of the circle of least confusion, Σ_{LC} [68]. The acoustic intensity should be high in this region since this is the part of the caustic that has the smallest diameter.

Three variables are required to determine the size and shape of a spherical reflector: the principal radius of curvature, R_r; the radius of the aperture, r_r; and the depth measured normal to the plane of the rim, x_r. To simplify the analysis, depth was constrained to be equal to $R_r/4$ in each case. (This constraint is the result of a trade-off between achieving good beam confinement and reducing the aberrations caused by diffraction at the rim of the reflector.) The variables R_r, r_r and x_r can be related to each other using Pythagoras' theorem ($r_r = \sqrt{2x_r R_r - x_r^2}$). Therefore, with the constraint that $x_r = R_r/4$, the reflector can be defined completely by just one variable; the radius of the aperture, r_r.

The acoustic source positions were selected such that the paraxial foci were produced at an arbitrarily chosen distance of 2 m from the back of each reflector using the lens-maker's formula (see appendix A, equation (A 7)). The longitudinal and transverse spherical aberrations (L_{SA} and T_{SA} respectively) for three different aperture radii are presented in table 1. Also shown is the angle θ_r measured at the sound source and subtended between the rim of a spherical reflector and the acoustic axis.

r_r (m)	Σ_{LC} (m)	L_{SA} (m)	T_{SA} (m)	θ_r (rad)
0.125	0.055	1.498	0.399	1.177
0.150	0.061	1.412	0.383	1.170
0.175	0.067	1.330	0.366	1.163

Table 1 *Simulation results for 25, 30 and 35 cm diameter spherical reflectors.*

It was expected that the larger the aperture, the larger the spherical aberration that would be observed. This is true if the position of the source is fixed relative to the back of the reflector. However, in this analysis (and in practice) it was the position of the focus that was fixed. It can be seen that both the longitudinal and the transverse spherical aberrations actually improve with the larger dish. The penalty, however, is that the source must be moved slightly farther from the reflector such that the angle, θ_r, reduces and the diameter of the circle of least confusion, Σ_{LC}, increases. Thus, the amount of power collected from the source reduces, as does the confinement of the beam in the circle of least confusion.

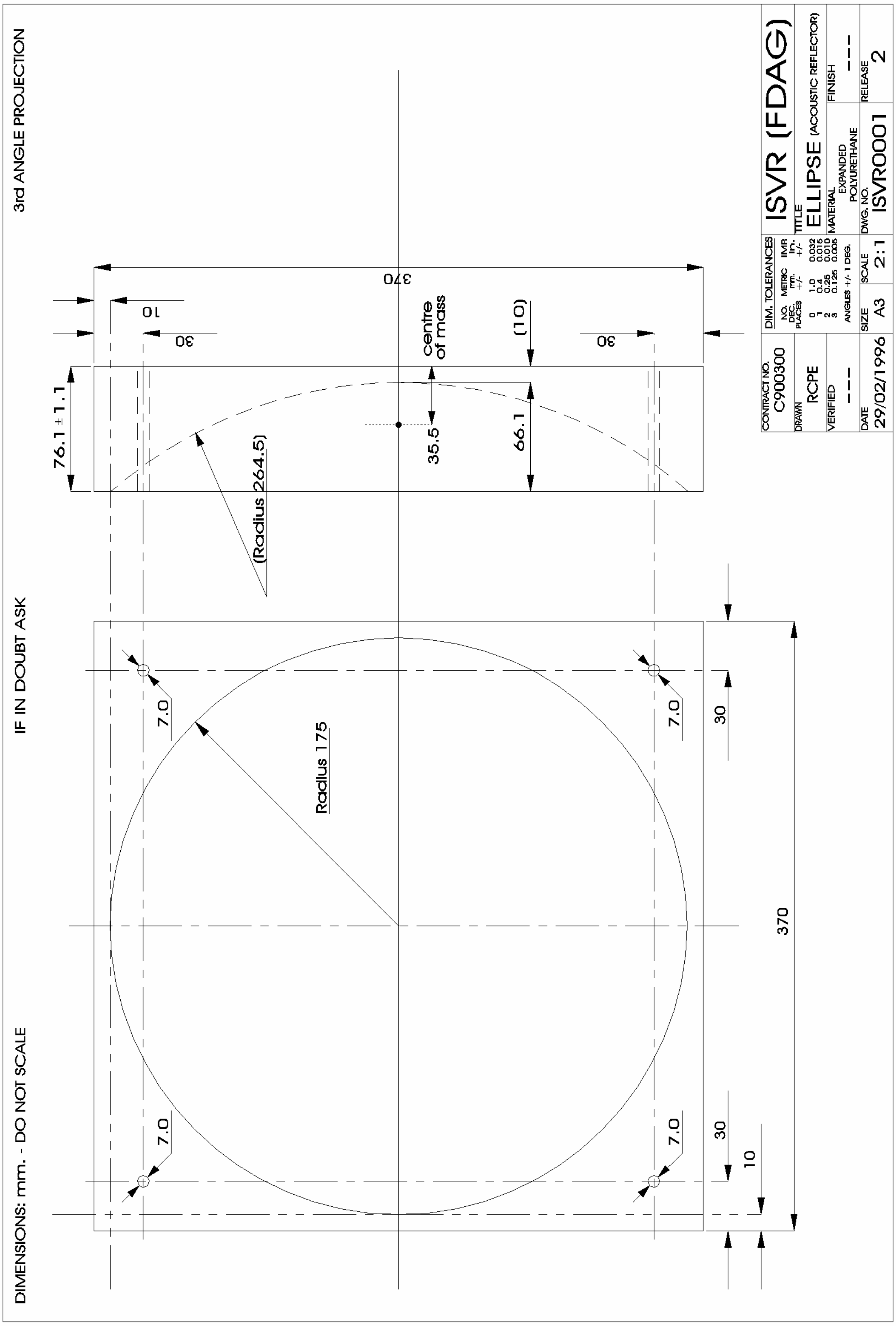

Figure 12 *The design specification for an acoustic reflector.*

Spherical aberration was considered to be a more important factor than confinement within the circle of least confusion. (The reason for this is better illustrated in a practical measurement, as shown in the next section.) Therefore, the larger, 35 cm diameter reflector size was chosen. Two such reflectors were cut from a block of closed-cell expanded polyurethane foam, according to the design specification shown in figure 12. To limit scatter, the surface tolerance was specified to be ± 1 mm, *i.e.*, around $^{1}/_{20}$ of an acoustic wavelength at 75 kHz in water.

The reflector material was chosen on the basis that the polyurethane frame would be robust enough to withstand handling whilst the air trapped within the closed pores would ensure a large acoustic impedance mismatch in water. Alternative reflector materials were also considered, but polyurethane foam was decided to be the best to use on the grounds of cost and the ease of fabrication.

Hydrophones were used as both the acoustic source and receiver elements. As noted in footnote 12, manufacturer's data indicates that the variation in their sensitivity should have been less than 3 dB in every direction at a frequency of 100 kHz or less [47]. In order to confine their directional responses to within the collection angles of the reflectors, back-reflectors were attached to each of the hydrophones.

3.2 Free-Field Characterisation

The performance of one of the reflectors was assessed when acting as an acoustic source. It was submerged in a large (8 m × 8 m × 5 m deep) water tank[14], which allowed side-wall reflections to be removed by time windowing. It proved very difficult to adjust the paraxial focus accurately because of the non-linear relationship between the focus and source positions. Therefore, the hydrophone was carefully positioned and fixed at a distance of S_0 = 13 cm from the back of the reflector such that the paraxial focus was, in theory, close to infinity. (This setup was maintained throughout all the subsequent experiments that involved the reflectors by the use of thin steel rods which held the hydrophones firmly in place.)

---

[14] The A B Wood Underwater Acoustics Facility at the University of Southampton, Institute of Sound and Vibration Research.

The hydrophone, when used as an acoustic projector, was driven by a series of single-cycle sine wave pulses, each having a centre frequency of 75 kHz (*cf.*, section 2.2.1 and footnote 9). The acoustic pressure amplitude that resulted from each pulse was recorded at discrete points in front of the reflector using an independent hydrophone.

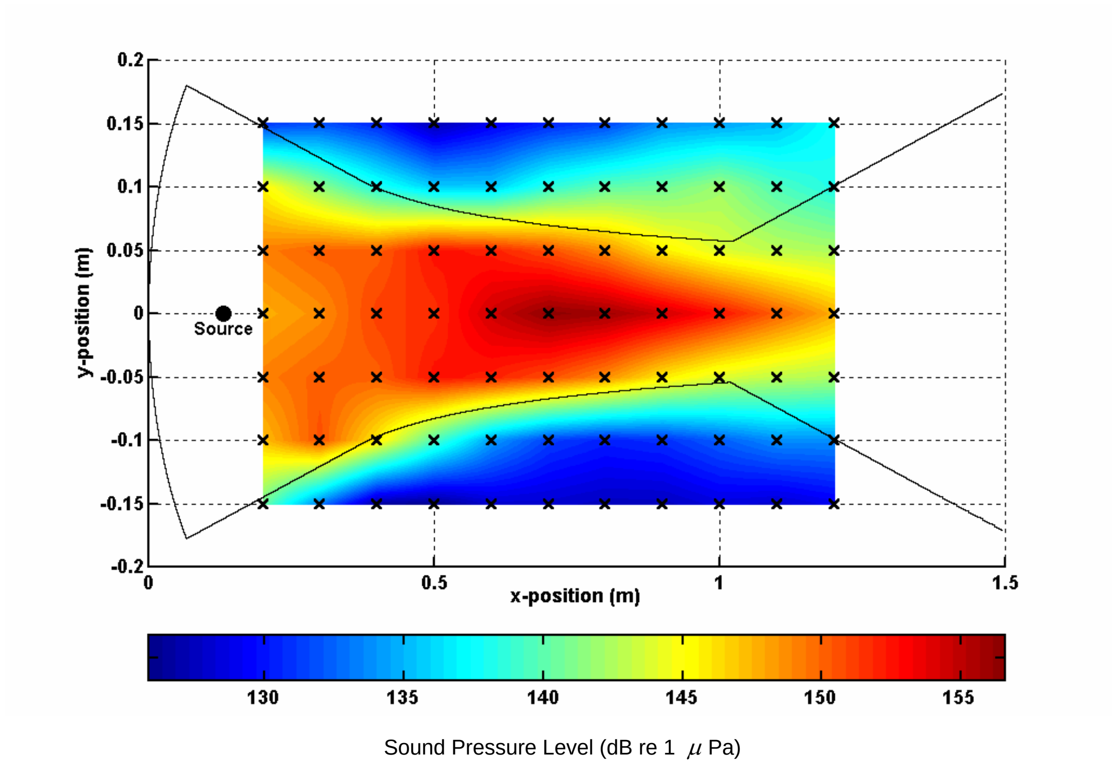

***Figure 13** The sound field generated by a focused acoustic reflector (focusing at ∞). The crosses represent discrete measurement positions and the solid line delineates the theoretical boundary of the acoustic field. (Original in colour.)*

The measured sound field is shown in figure 13. The value at each of the sample points, ×, is the intensity level, IL; the pulse-averaged intensity measured at the receiver, I_{pa}, divided by a reference intensity, I_{ref}, and expressed using a logarithmic scale, $IL = 10\log_{10}\left(I_{pa}/I_{ref}\right)$ dB re I_{ref}. This is the same as the sound pressure level for an equivalent plane or spherical wave, *i.e.*, $SPL = 20\log_{10}\left(P_e/P_{ref}\right)$ dB re P_{ref}, where P_e is an effective pressure and P_{ref} is a reference pressure [69, 70]. A continuous image was obtained using piecewise, bilinear interpolation between the sampling points. The solid outline delineates the theoretical boundary of the acoustic field, *i.e.*, the back of the reflector and the caustic.

It can be seen that the highest energy density coincides with the point at which marginal rays cross the acoustic axis, *i.e.*, the position of the L_{SA}. (It should be noted that the ray tracing model is, at best, an approximation for marginal rays, since diffraction effects are most severe at the rim of the reflector.) The L_{SA} associated with the smaller reflectors (see table 1) would have caused the high energy region to be closer to the acoustic projector. Therefore the choice of the larger, 35 cm diameter reflector proved to be the most appropriate for producing a high energy density at the greatest range in the medium.

A quantity known as the directivity index is often used to measure the performance of an acoustic source [57]. It is defined as the ratio of the intensity of a directional source at some distance on the acoustic axis to the intensity of a simple (omni-directional) source at the same distance. The directivity index of the focused acoustic reflector was estimated to be greater than 20 dB from the data shown in figure 13 and from a measurement of the intensity of an unfocused source at the same distance as the circle of least confusion of the focused source.

3.3 Transmission Loss

The transmission loss associated with a focused acoustic beam propagating in the sediment was investigated using a reflector / hydrophone used as an acoustic source, Tx, and an independent hydrophone acting as a receiver, Rx. The water-sediment interface was given to be flat such that sound would be transmitted into the sediment in the same way, regardless of where it was projected on the interface.

For this assumption to be valid, it was necessary for the interface to display translational invariance, or stationarity, such that the statistics of one section of the surface were the same as the statistics of a different section of the same surface [71]. This property is commonly displayed by random, rough surfaces, and is mathematically essential for studies of wave scattering where the scattered field is regarded as a statistical quantity. (The nature of the sediment interface and its effect on wave scattering is dealt with in a subsequent report[4].)

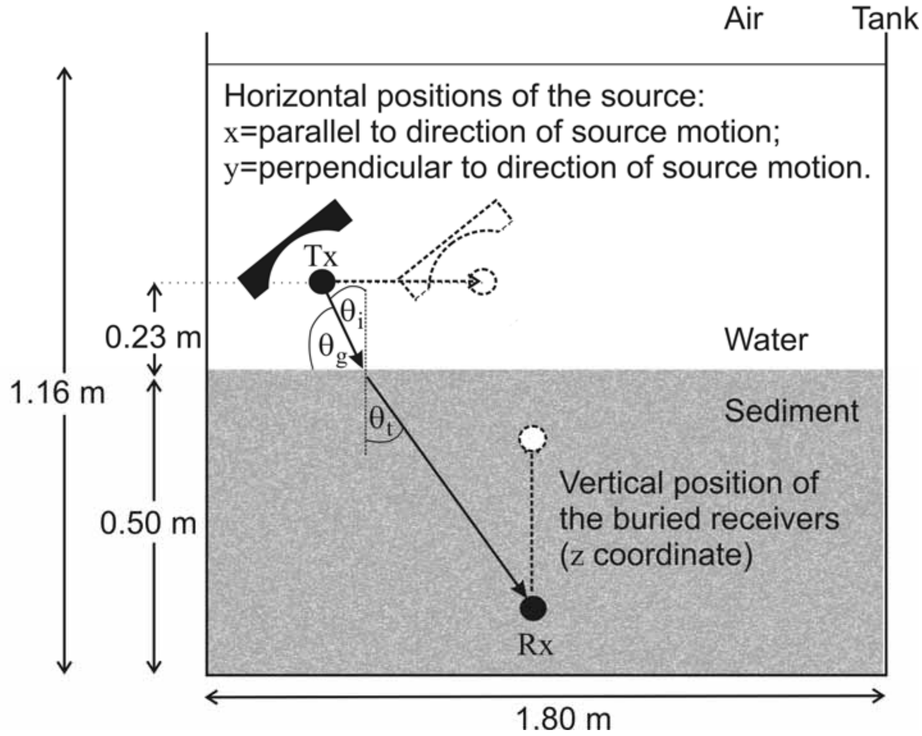

Figure 14 *The source / receiver arrangement for the sediment transmission loss measurement in the laboratory tank. The filled symbols represent the initial positions of the acoustic source, Tx, and receiver, Rx. The outlined symbols represent the range of positions of Tx and Rx.*

Hence, it was possible to obtain a two-dimensional measurement by moving the receiver vertically (*i.e.*, in the *z*-direction) within the sediment and the reflector horizontally (*i.e.*, in the *x*-direction) above it. This approach caused less disturbance to the sediment than would have been the case if the source was kept at a fixed position and the receiver was moved horizontally as well as vertically. The source / receiver arrangement is shown in figure 14.

In order to achieve reasonable coverage of the sediment volume in range and in depth (when moving the transducers in the horizontal plane) it was estimated that the acoustic axis of each reflector would have to be incident on the sediment bed at an angle of around 30°. In practice it was necessary to mount the reflector very rigidly and the method used did not allow adjustment over a continuous range of angles. The best that could be achieved was an angle of incidence, θ_i, measured to be 33° ± 2°.

Using Snell's law (equation (10)) and the sound speeds measured in section 2.2.1, the angle of transmission, θ_t, was predicted to be 38.6° ± 2.8°.

From the free-field measurement of the reflector sound field (figure 13), a suitable height for the hydrophones was estimated to be around 25 cm above the sediment surface. This should have resulted in the region of highest sound pressure being located at a depth of around 25 cm beneath the sediment surface. After having completed the final adjustments to the apparatus, the height of each of the hydrophones was measured to be 23 cm ± 1 cm.

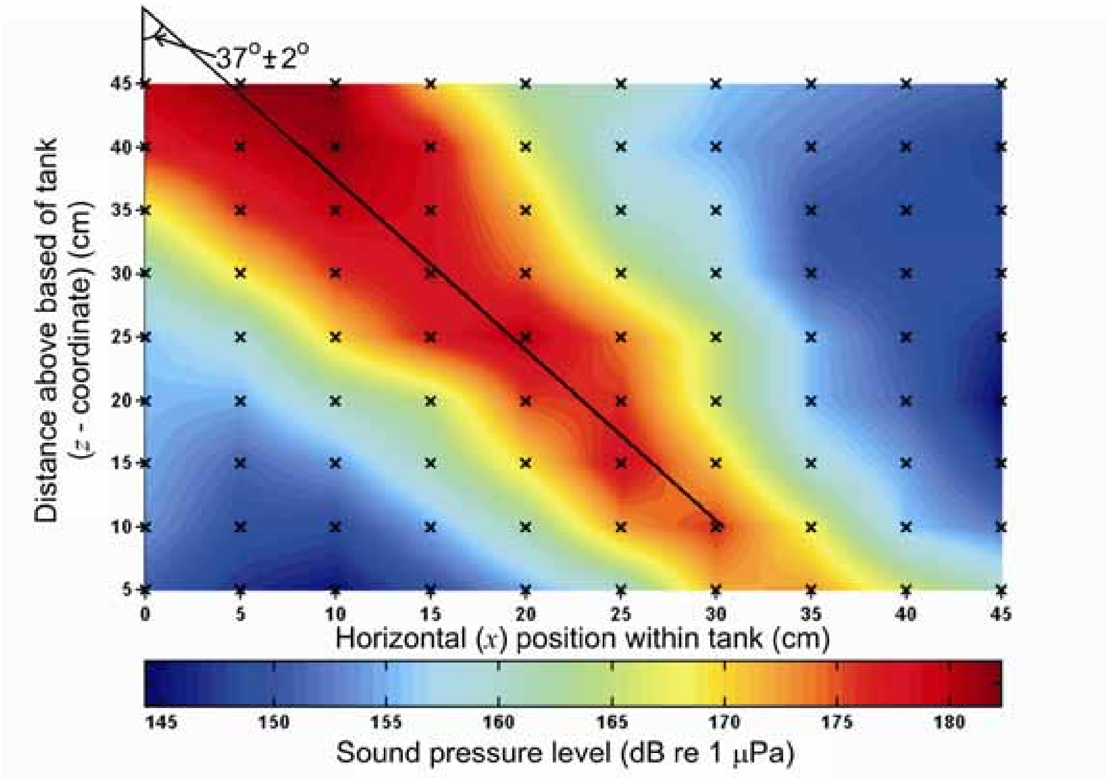

***Figure 15** The sound field generated within the sediment bed by a focused acoustic reflector. The crosses represent discrete measurement positions. The solid line indicates the calculated position of the acoustic axis. (Original in colour.)*

The acoustic projector was driven by a series of single-cycle sine wave pulses, each having a centre frequency of 75 kHz (*cf.*, section 2.2.1 and footnote 9). The transmission loss, shown in figure 15, was obtained by interpolating between measurements recorded at various sample points, ×, within the sediment. The value at each point is the sound pressure level for an equivalent plane or spherical wave, as described section 3.2.

The direction of the acoustic axis was calculated as follows: The sample point having the maximum value of sound pressure level was found at every sample depth. These were plotted to give a series of points that were equally-spaced in depth, but unequally-spaced in range. A straight line was fitted to these points and its gradient, *i.e.*, the gradient of the acoustic axis, was determined. The angle of transmission, θ_t, was found to be 37° ± 2°, which is in agreement with the predicted value.

With reference to the measurements in sand, the plane-wave attenuation coefficient in the laboratory sand at a frequency of 75 kHz was known to be 31 dB m^{-1} ± 2.5 dB m^{-1}. With reference to figure 15, however, the attenuation on the acoustic axis was observed to be much lower than this value, being around 19 dB m^{-1}. This difference is attributed to the geometric focusing of acoustic energy from the source by the reflector. Converging wavefronts on the acoustic axis give rise to enhanced penetration. (It has been noted that hydrophones are not intended for use in sediment and, therefore, these measurements should be treated with some caution. For measurements in this study where hydrophones calibrated in-water are used in sediment, the insertion loss error was estimated to be around ± 1 dB.)

4 The Automated Control System

An automated position control rig was constructed (shown in figure 16) to simplify the acquisition of data from a large number of sample points within the sediment. A rectangular frame with two independent sliding beams was mounted above the laboratory tank. A sliding stage was attached to each beam, below which the acoustic reflectors were suspended. All the components of the rig near to the water were made from anodised aluminium and stainless steel to minimise corrosion. Dissimilar metals were prevented from coming into contact to prevent galvanic corrosion [72].

A stepper-motor and gearbox assembly was attached to each of the four sliding elements, allowing the reflectors to be positioned anywhere in the two-dimensional plane above the sediment. The assembly was designed to be as stable as possible, with the centres of mass of each of the buoyant reflectors centrally positioned to evenly distribute stresses within the frame. The height and orientation of the reflectors was fixed so that they always remained pointing in the same direction. Slack in the gearbox resulted in a small error of up to ± 1 cm about the programmed position. The error in the mean position of the sliding elements was measured to be less than 1 cm over a travel length of 150 cm.

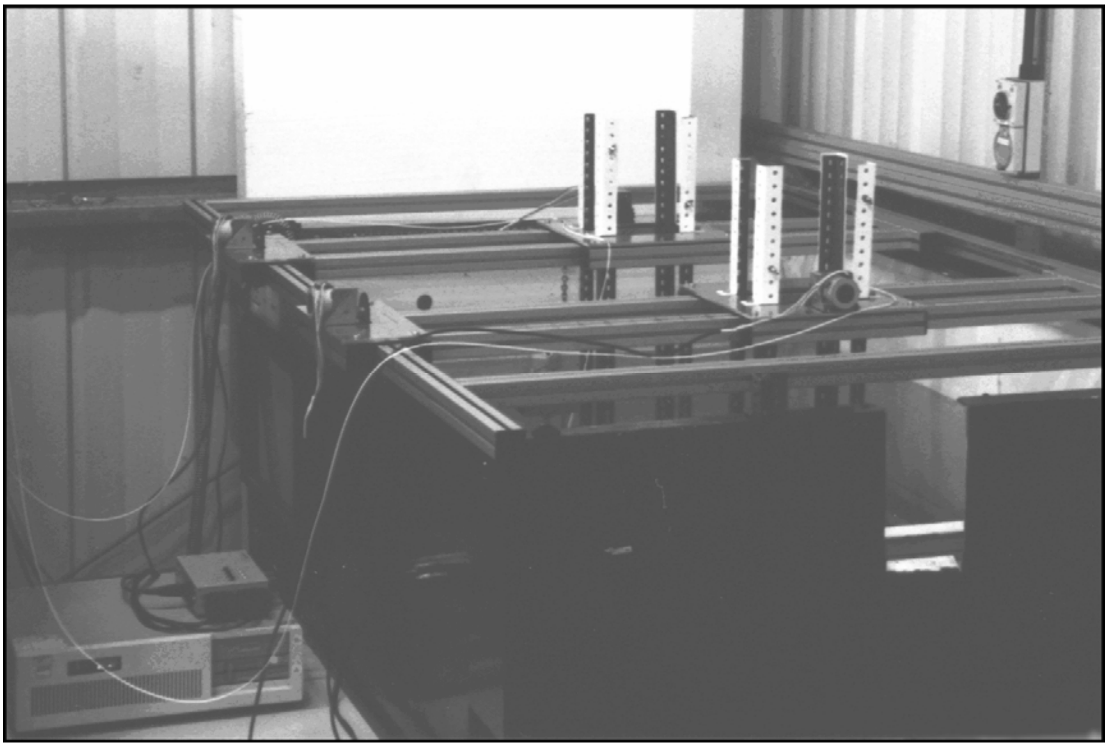

Figure 16 *The position control rig mounted above the laboratory tank.*

A dedicated computer, host to four stepper-motor control boards, and a separate power supply were used to drive the motors. Control commands were sent from a second, more powerful computer via an RS-232 null modem link. The second computer was used to co-ordinate the entire signal generation / data acquisition process. It was equipped with a DAQ card that was used for both data acquisition and signal generation, and a GPIB card that enabled the remote control of a fast digital storage oscilloscope. The basic arrangement of the signal generation / data acquisition hardware is shown in figure 17.

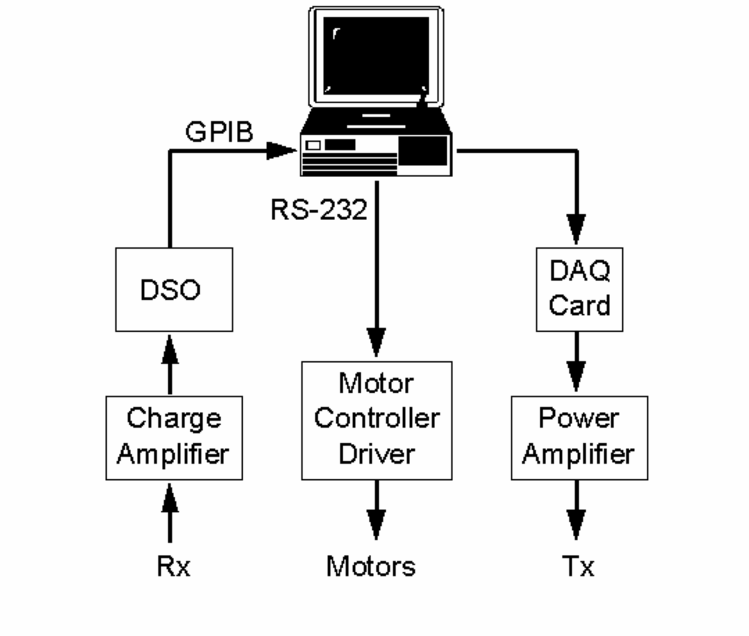

Figure 17 *The arrangement of the signal generation / data acquisition hardware that was used in the laboratory tank automated control system.*

Control software for the acquisition card, the oscilloscope and the stepper-motors was written using the LabView™ programming environment. A standard file format was adopted so that waveform data could be exported to other software packages, particularly MatLab™, for post-processing and analysis.

Discrete positions were calculated for the acoustic transducers, such that the reflector beams intersected at a range of points in the middle of each xz-plane. In the example shown in figure 18, the height and orientation of the transducers corresponds to the arrangement described in section 3.3. That is to say, the hydrophones were positioned 23 cm above the sediment surface, the reflectors were inclined at 33° ± 2°, and the angle of transmission into the sediment was 37° ± 2°.

The symbols, + and ×, correspond to the positions of the two hydrophones (acoustic projector and receiver, respectively). Acoustic beams projected into the sediment from these positions intersect at the 60 sample points marked by the symbols, o. These points cover an area 20 cm wide and 30 cm deep in the centre of the xz-plane. An example for one combination of source and receiver positions is indicated in the figure. By moving the transducers in the *y*-direction, *i.e.*, out of the plane of the paper, it was possible to scan successive planes and, thereby, sample a three-dimensional volume within the sediment.

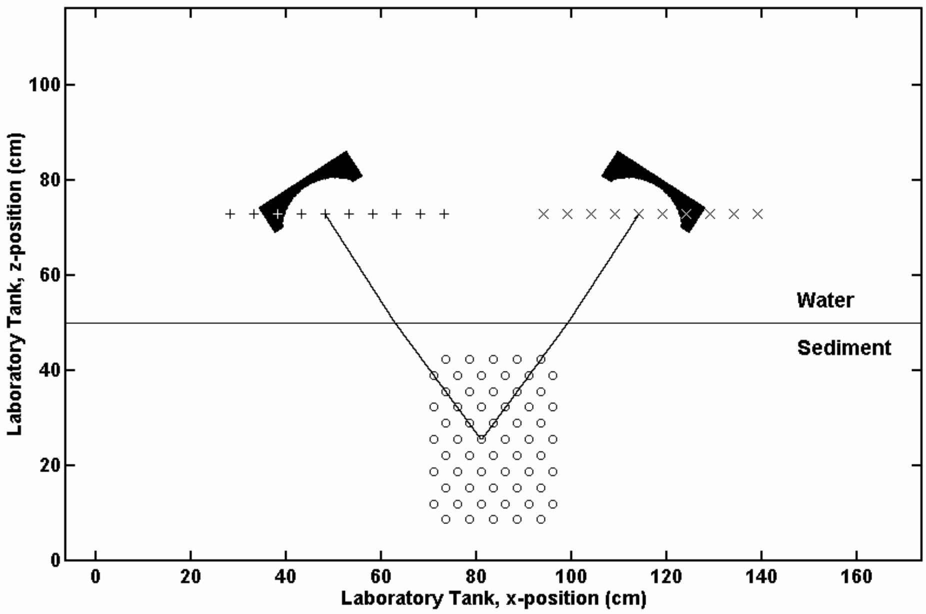

Figure 18 *An example scanning pattern for the automated position control system, as viewed from the side of the laboratory tank. Symbols: + = discrete positions of the acoustic projector;* × *= discrete positions of the acoustic receiver;* o *= points of intersection within the sediment.*

5 Summary

In this report, the construction of a laboratory-scale test facility has been described. It was intended that the physical and acoustical properties of the laboratory system should be similar to those found in a real seafloor environment. In particular, the tank should represent the type of environment in which a submarine cable detection system is required to operate. A transducer system was also described, which was suitable for an investigation into the non-invasive acoustic detection of buried objects. Several parameters have been determined in this report that pertain to the acoustical characteristics of the water and sediment in the laboratory tank in the 10 – 100 kHz frequency range. These parameters are summarised in table 2.

Parameter	Value
Sediment grain density	2 670 kg m^{-3} ± 2.5 %
Density of the water in the tank	1 000 kg m^{-3} ± 0.1 %
Bulk density of the sediment	2 110 kg m^{-3} ± 2.5 %
Porosity of the sediment	~ 0.33
Speed of sound of the water in the tank	1 478 m s^{-1} ± 2 %
Speed of sound in the sediment	1 692 m s^{-1} ± 2 %
Attenuation coefficient in the sediment	$0.41 f_k^1$ dB m^{-1}
Directivity index of the focused source	> 20 dB

Table 2 A summary of the parameters identified in this report.

The laboratory tank was part-filled with a fine, angular-grained sand, with special consideration being given to the removal of gas bubbles. Sound speed and attenuation were identified as being critical parameters, requiring particular attention. Hence, these were investigated separately for each component of the acoustic path.

The attenuation in water and suspensions at 100 kHz was found to be less than 0.1 dB m^{-1} in both cases. Conversely, the attenuation in the sediment was greater than 10 dB m^{-1} for the frequency range of interest in this investigation. Only the attenuation in the sediment was considered to be significant. This means that the sound pressure developed by the source must be high enough to penetrate to the required depth within the sediment. However, caution must be exercised to ensure that reverberant energy does not dominate at the receiver. Therefore, a narrow beamwidth was also specified.

A focused reflector was considered to be the most cost-effective way of achieving a high acoustic power and narrow beamwidth. A comparison of different reflector sizes suggested that a larger aperture would result in less spherical aberration, thus producing a more uniform sound field. Diffraction effects were kept to a minimum by specifying a tolerance of much less than an acoustic wavelength over the reflector surface. The free-field performance of the transducers was found to be in agreement with the model prediction.

The transmission loss associated with an acoustic beam penetrating into the sediment was measured. The angle of transmission was found to be in good agreement with the value calculated using Snell's law (given the assumption of a smooth, flat sediment surface). However, the effective attenuation on the acoustic axis of the transducer was found to be significantly less than the plane wave attenuation observed in similar sediments. This enhancement in penetration was explained as being due to the geometric focusing of the acoustic beam by the reflector.

An automated control system was developed to simplify the data acquisition process. This was, primarily, a motor-driven position control system which allowed the transducers to be accurately positioned in the two-dimensional plane above the sediment. Thus, it was possible for the combined signal generation, data acquisition and position control process to be co-ordinated from a central computer.

In the introduction to this report, the importance of ensuring that useful results could be obtained from a scaled-down laboratory system was noted. The most significant difference between the laboratory and the field was the depth of burial that could be achieved. With only 50 cm of sediment available, the maximum burial depth was between 25 and 30 cm, whereas telecommunication cables are buried up to 1 m deep.

Provided that a high sound pressure level and narrow beamwidth can be maintained by a transducer system over the longer path length, similar results may be obtainable simply by increasing the acoustic power of the source. Ordinarily, an increase in the power of the source would lead to an unacceptable increase in the reverberation level within the sediment. However, the narrow source beamwidth and the use of time-gating (which is explored in a later report tin this series[6]) mitigates this effect.

The scattering of acoustic energy at the rough water-sediment interface is important. It is difficult to say whether or not this will significantly affect the performance of an acoustic detection system. (There has been vigorous debate in academic circles over the very nature of the transmission of acoustic energy within the sediment.) Therefore, the scattering of acoustic energy incident on a rough water-sediment interface is investigated in the next report in this series[4]. An experimental study into the effect of roughness on the transmission of sound into the sediment in the laboratory tank is also presented. This material formed the basis of the PhD of RCPE [73-76].

APPENDIX A

THE DESIGN OF AN ACOUSTIC REFLECTOR

A.1 Calculation of the Paraxial Focus

An acoustic source / reflector arrangement is shown in figure A 1. The principal radius of curvature of the spherical reflector is denoted by R_r. The source is positioned on the axis at a distance, S_0, from the back of the reflector, O. Rays hitting the reflector intercept the axis at a distance S_i from O. (An example of a marginal ray is shown in the diagram.)

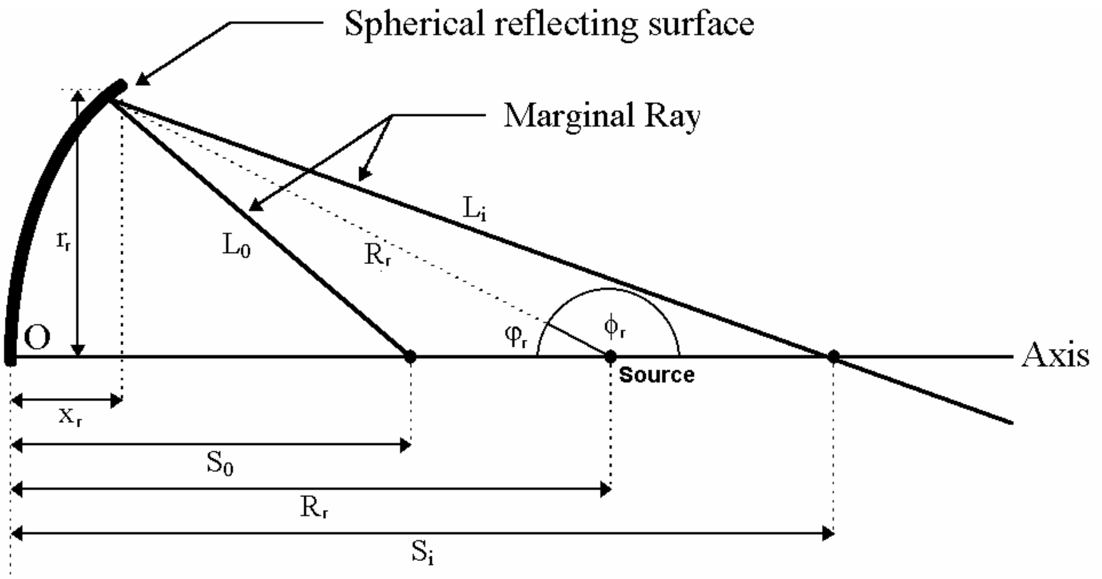

Figure A 1 *An acoustic source and a section of a spherical reflector. The path of a marginal ray from the source,* S_0*, to the axial-intercept,* S_i*, is shown.*

The optical path length, OPL, is defined as

$$\mathrm{OPL} = L_0 + L_i \tag{A 1}$$

It can be shown that

$$L_0 = \left[R_r^2 + \left(R_r - S_0\right)^2 - 2R_r\left(R_r - S_0\right)\cos\varphi_r\right]^{\frac{1}{2}} \tag{A 2}$$

and given that

$$\cos\phi_r = -\cos\varphi_r \quad ; \; \phi_r = \left(\pi - \varphi_r\right) \tag{A 3}$$

it follows that

$$L_i = \left[R_r^2 + \left(S_i - R_r\right)^2 + 2R_r\left(S_i - R_r\right)\cos\varphi_r\right]^{\frac{1}{2}} \tag{A 4}$$

Using Fermat's principle of least time [77] which states,

$$\frac{d(OPL)}{d\varphi_r} = 0 \tag{A 5}$$

it follows that

$$\begin{gathered} \frac{1}{2L_0}\left[2R_r\left(R_r - S_0\right)\sin\varphi_r\right] + \frac{1}{2L_i}\left[-2R_r\left(S_i - R_r\right)\sin\varphi_r\right] = 0 \\ \therefore \frac{R_r - S_0}{L_0} + \frac{R_r - S_i}{L_i} = 0 \end{gathered} \tag{A 6}$$

In the paraxial region,

$$\begin{gathered} \cos\varphi_r \to 1 \\ S_0,\; S_i \to L_0,\; L_i \\ \therefore \frac{1}{S_0} + \frac{1}{S_i} = \frac{2}{R_r} \end{gathered} \tag{A 7}$$

which is known as the lens-maker's formula [78].

For non-paraxial rays, Pythagoras' theorem is used:

$$\begin{gathered} x_r = \sqrt{R_r^2 - R_r^2\cos^2\varphi_r} \\ \therefore \cos\varphi_r = \sqrt{1 - \left(\frac{x_r}{R_r}\right)^2} \end{gathered} \tag{A 8}$$

The parameters R_r, S_0 and L_0 are a constant for a given acoustic reflector. Therefore for a given reflector we may define a parameter $\varsigma = (R_r - S_0)/L_0$ which is a constant for that reflector. The objective is to find the axial intercept, S_0, for any given angle of an acoustic "ray" from the source, φ_r. Substituting L_i from equation (A 4) into equation (A 6), $\varsigma = (R_r - S_0)/L_0$ becomes:

$$\varsigma = \frac{R_r - S_0}{L_0} = \frac{S_i - R_r}{\left[R_r^2 + (S_i - R_r)^2 + 2R_r(S_i - R_r)\cos\varphi_r\right]^{\frac{1}{2}}} \tag{A 9}$$

The solution of equation (A 9) gives S_i for any φ_r given the reflector constants (R_r, S_0 and L_0). This can be found by rearranging equation (A 9) into quadratic form,

$$\left(\varsigma^2 - 1\right)S_i^2 + 2R_r\left[\varsigma^2(\cos\varphi_r - 1) + 1\right]S_i - R_r^2\left[2\varsigma^2(\cos\varphi_r - 1) + 1\right] = 0 \tag{A 10}$$

and solving for the secondary focus, S_i. (One of the two roots will also give the distance from O to the primary focus, S_0.)

A.2 Spherical Aberration

Spherical aberration corresponds to a dependence of focal length on aperture for non-paraxial rays [79]. For the converging reflector shown in figure A 1, marginal rays are focused in front of paraxial rays. The distance between the axial intersection of a marginal ray (from equation (A 10)) and the intersection of a paraxial ray (from equation (A 7)) is known as the longitudinal spherical aberration, or L_{SA}. Similarly, the height at which a marginal ray passes above the paraxial focus is known as the transverse spherical aberration, or T_{SA}. These are illustrated in figure A 2.

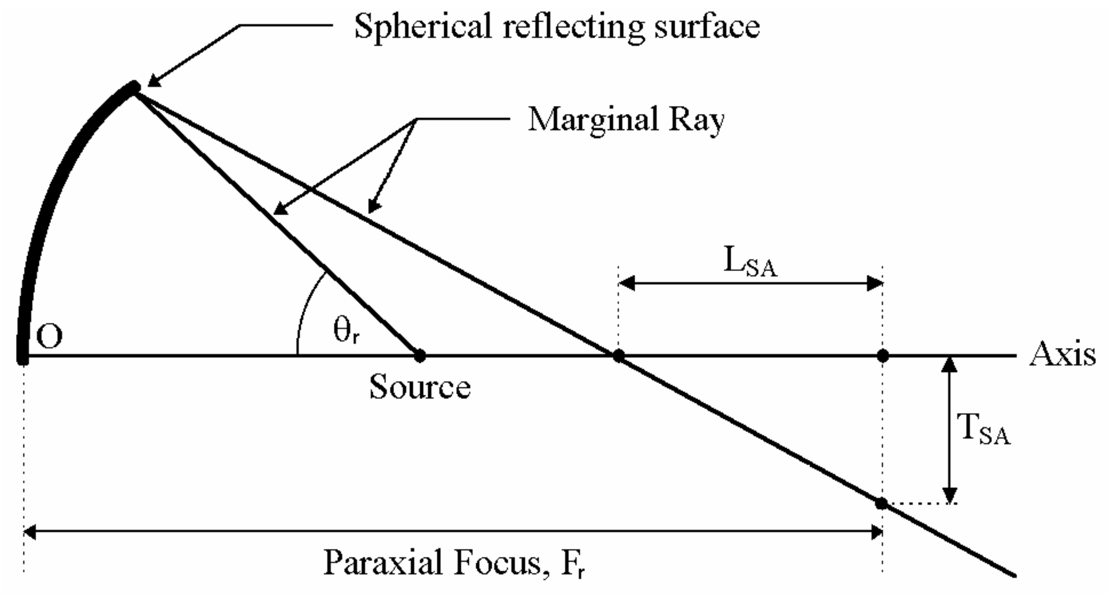

Figure A 2 *The longitudinal and transverse spherical aberrations associated with a spherical reflector.*

The spherical aberration can be reduced by stopping down the aperture but this also has the effect of reducing the amount of power entering the system. The collection angle, θ_r, allows a comparison to be made of the power gathering capability of different source / reflector arrangements.

With reference to figures A 1 and A 2, the longitudinal spherical aberration is

$$L_{SA} = \left| F_r - S_i \right| \tag{A 14}$$

and the transverse spherical aberration is

$$T_{SA} = \left| \left(L_{SA} - x_r \right) \left(\frac{r_r}{F_r - x_r} \right) \right| \tag{A 15}$$

A.3 Modelling the Caustic

Ray tracing is often an excellent method for modelling specular scatter in a cluttered environment. Several ray paths have been traced out, using the preceding equations, to produce the caustic shown in figure A 3. (For clarity, the rays have been shown from the point of reflection onwards.) The circle of least confusion (which has diameter Σ_{LC}) is the best place to observe an image [80]. For the acoustic reflector, the intensity of the beam is greatest in this region.

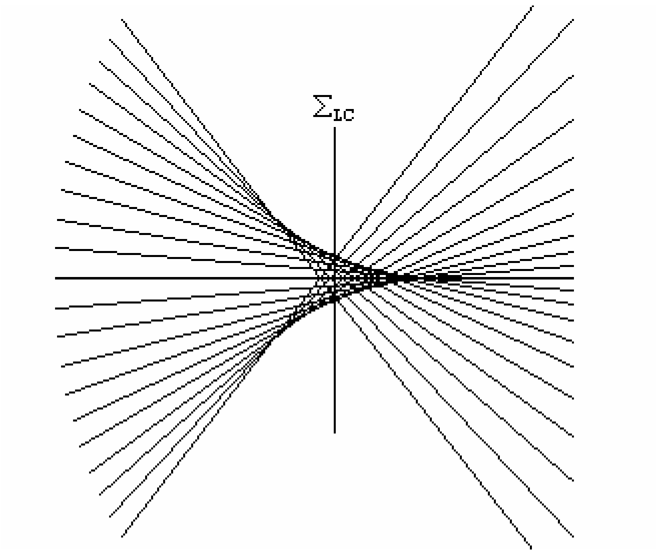

Figure A 3 *A ray-traced caustic illustrating the circle of least confusion,* Σ_{LC}.

Ray tracing can be inadequate when small diffractors with a correlation length less than a wavelength are present. For the acoustic reflector, the discontinuity at the rim will cause diffraction that will not be reproduced by the ray tracing model. This is equally true if the surface tolerance of the reflector is not smooth to within much less than a wavelength.

References

[1] Apel J R, *Principles of Ocean Physics*, (International Geophysics Series, Volume 38), Academic Press, 1987.

[2] Hamilton E L, “Compressional-wave attenuation in marine sediments”, *Geophysics*, pp. 620 - 646, August 1972.

[3] Thorne P D, Campbell S C, “Backscattering by a suspension of spheres”, *Journal of the Acoustical Society of America*, Volume 92, Number 2, Part 1, pp. 978 - 986, August 1992.

[4] Nyborg W L, Rudnick I, Schilling H K, “Experiments on acoustic absorption in sand and soil”, *The Journal of the Acoustical Society of America*, Volume 22, Number 4, pp. 422 - 425, July 1950.

[5] Kinsler L E, Frey A R, Coppens A B, Sanders J V, *Fundamentals of Acoustics*, 3rd Edition, John Wiley & Sons, Inc, Toronto, Appendix 10, 1982.

[6] Hamilton E L, “Elastic Properties of Marine Sediments”, *Journal of Geophysical Research*, Volume 76, Number 2, pp. 579 - 604, January 10, 1971.

[7] Leighton T G, *The Acoustic Bubble*, Academic Press Ltd, London, Chapter 2, pp. 78 - 83, 1994.

[8] Pickard G L, Emery W J, *Descriptive Physical Oceanography: An Introduction*, 4th (SI) Edition, p. 11, Pergamon Press, 1982.

[9] Zabrodsky S S, *Hydrodynamics and Heat Transfer in Fluidised Beds*, The M.I.T. Press, 1966.

[10] Boyle F A, Chotiros N P, “Nonlinear acoustic scattering from a gassy poroelastic seabed”, *Journal of the Acoustical Society of America*, Volume 103, Number 3, pp. 1328 - 1336, March 1998.

[11] Goff J A, Jordan T H, “Stochastic Modeling of Seafloor Morphology: Inversion of Sea Beam Data for Second-Order Statistics”, *J. Geophys. Res.*, Vol. 93, No. B11, pp. 13589 - 13608, November 10, 1988.

[12] Hecht E, *Optics*, 2nd Edition, Addison-Wesley Publishing Company, Chapter 14, pp. 559 - 562, 1987.

[13] Hecht E, *Optics*, 2nd Edition, Addison-Wesley Publishing Company, Chapter 10, p. 419, 1987.

[14] McLane M, *Sedimentology*, Chapter 2, p. 14, Oxford University Press, Inc., 1995.

[15] Urick R J, *Principles of Underwater Sound*, McGraw-Hill, New York, 3rd Edition, Section 5.4, pp. 111 - 116, 1983.

[16] Leroy C C, “Development of Simple Equations for Accurate and More Realistic Calculation of the Speed of Sound in Sea Water”, *Journal of the Acoustical Society of America*, Volume 46, p. 216, 1969.

[17] Leroy C C, Parthiot F, “Depth-pressure relationships in the oceans and seas”, *J. Acoust. Soc. Am.*, Vol. 103, No. 3, pp. 1346 - 1352, March 1998.

[18] Leighton T G, *The Acoustic Bubble*, Academic Press Ltd, London, Chapter 3, Section 3.8, 1994.

[19] Leighton T G, “Fundamentals of underwater acoustics” (Fahy F, Walker J, *Fundamentals of Noise and Vibration*, E & FN Spon, London and New York, 1998).

[20] Urick R J, *Principles of Underwater Sound*, McGraw-Hill, New York, 3rd Edition, Section 5.5, pp. 116 - 120, 1983.

[21] Brekhovskikh L M, *Waves in Layered Media*, 2nd Edition, Chapter 1, pp. 48 - 50, Academic Press, 1980.

[22] Hovem J M, “Attenuation of sound in marine sediments”, Electronics Research Laboratory, University of Trondheim, NorwayRayleigh, *The Theory of Sound*, Dover Publications, Inc., Chapter XIII, Section 270, 1945.

[23] Urick R J, *Principles of Underwater Sound*, McGraw-Hill, New York, 3rd Edition, p. 31, 1983.

[24] Kinsler L E, Frey A R, Coppens A B, Sanders J V, *Fundamentals of Acoustics*, 3rd Edition, John Wiley & Sons, Inc, Toronto, Chapter 5, pp. 105 - 107, 1982.

[25] Hamilton E L, “Acoustic Properties of Sediments”, *Acoustics and Ocean Bottom*, edited by A. Lara-Saenz, C. Ranz Guerra, and C. Carbofite (Consejo Superior de Investigaciones Cientificas (CSIC), Madrid (1987)).

[26] Rayleigh, *The Theory of Sound*, Dover Publications, Inc., Chapter XIX, Section 347, 1945.

[27] Mason W P (ed.), *Physical Acoustics*, Volume II, Part A, pp. 293 - 295, Academic Press.

[28] Kinsler L E, Frey A R, Coppens A B, Sanders J V, *Fundamentals of Acoustics*, 3rd Edition, John Wiley & Sons, Inc, Toronto, Chapter 7, pp. 157 - 160, 1982.

[29] Fisher F H, Simmons V P, “Sound absorption in sea water”, *Journal of the Acoustical Society of America*, Volume 62, Number 3, pp. 558 - 564, September 1977.

[30] Lyman J, Fleming R H, “Composition of sea water”, *Journal of Marine Research*, Volume 3, Number 2, pp. 134 - 146, 1940.

[31] Urick R J, *Principles of Underwater Sound*, McGraw-Hill, New York, 3rd Edition, Section 5.3, pp. 102 - 111, 1983.

[32] Urick R J, “The Absorption of Sound in Suspensions of Irregular Particles”, *Journal of the Acoustical Society of America*, Volume 2, Number 3, May 1948.

[33] Kinsler L E, Frey A R, Coppens A B, Sanders J V, *Fundamentals of Acoustics*, 3rd Edition, John Wiley & Sons, Inc, Toronto, Section 15.11, 1982.

[34] Pierce A D, *Acoustics: An Introduction to Its Physical Principles and Applications*, McGraw-Hill Book Company, pp. 428 - 429, 1981.

[35] Hickling R, “Analysis of Echoes from a Solid Elastic Sphere in Water”, *Journal of the Acoustical Society of America*, Volume 34, Number 10, pp. 1582 - 1592, October 1992.

[36] Richards S D, Heathershaw A D, Thorne P D, “The effect of suspended particulate matter on sound attenuation in seawater”, *Journal of the Acoustical Society of America*, Volume 100, Number 3, September 1996.

[37] Johnson R K, “Sound scattering from a fluid sphere revisited”, *Journal of the Acoustical Society of America*, Volume 61, Number 2, pp. 375 - 377, February 1977.

[38] Sheng J, Hay A E, “An examination of the spherical scatterer approximation in aqueous suspensions of sand”, *Journal of the Acoustical Society of America*, Volume 83, Number 2, pp. 598 - 610, February 1988.

[39] Sun S, Thorne P D, Bjørnø I K, Mazoyer T, "Observations of acoustic backscattering by elastic cubes", *Proceedings of the 3rd European Conference on Underwater Acoustics*, Heraklion, Crete, Greece, pp. 51 - 56, 1996.

[40] Richards S D, Brown N R, Leighton T G, "Characteristion of Propagation Parameters for High Frequency Sonar in Turbid Coastal Waters", *Proceedings of the 4th European Conference on Underwater Acoustics*, Rome, Italy, pp. 709 - 714, 1998.

[41] Brown N R, Leighton T G, Richards S D, Heathershaw A D, "Measurement at 50 - 150 kHz of Absorption due to Suspended Particulate Matter", *Proceedings of the 16th International Congress on Acoustics and 135th Meeting of the Acoustical Society of America*, Seattle, Washington, USA, pp. 1347 - 1348, 1998.

[42] Richards S D, "The effect of temperature, pressure, and salinity on sound attenuation in turbid seawater", *Journal of the Acoustical Society of America*, Volume 103, Number 1, pp. 205 - 211, January 1998.

[43] Clay C S, Medwin H, *Acoustical Oceanography; Principles and Applications*, John Wiley & Sons, New York, p.260, 1977.

[44] Pierce A D, *Acoustics: An Introduction to Its Physical Principles and Applications*, McGraw-Hill Book Company, pp. 111 - 113, 1981.

[45] Hamilton E L, "Sound attenuation as a function of depth in the sea floor", *J. Acoust. Soc. Am.*, Vol. 59, No. 3, pp. 528 - 535, March 1976.

[46] Nielsen R O, *Sonar Signal Processing*, Artech House, Inc., p.199, 1991.

[47] Brüel & Kjær, Technical Documentation for Hydrophone Types 8103, 8104, 8105, 8106, March 1992.

[48] Pierce A D, *Acoustics: An Introduction to Its Physical Principles and Applications*, McGraw-Hill Book Company, pp. 352 - 353, 1981.

[49] Urick R J, *Principles of Underwater Sound*, McGraw-Hill, New York, 3rd Edition, Section 5.8, pp. 136 - 143, 1983.

[50] Rayleigh, *The Theory of Sound*, Dover Publications, Inc., Chapter XIII, Section 270, 1945.

[51] Brekhovskikh L M, Lysanov Y P, *Fundamentals of Ocean Acoustics,* Second Edition, Chapter 3, Springer-Verlag, 1991.

[52] Kinsler L E, Frey A R, Coppens A B, Sanders J V, *Fundamentals of Acoustics*, 3rd Edition, John Wiley & Sons, Inc, Toronto, Chapter 6, 1982.

[53] Pain H J, *The Physics of Vibrations and Waves*, 4th Edition, John Wiley & Sons Ltd, pp. 235 - 240, 1995.

[54] Boyle F A, Chotiros N P, "A model for acoustic backscatter from muddy sediments", *Journal of the Acoustical Society of America*, Volume 98, Number 1, July 1995.

[55] IUSD Sonar Survey, *International Underwater Systems Design*, A. P. Publications, Ltd, Volume 19, Number 4, pp. 12 - 21, July / August 1997.

[56] Urick R J, *Principles of Underwater Sound*, McGraw-Hill, New York, 3rd Edition, Chapter 4, pp. 75 - 79, 1983.

[57] Kinsler L E, Frey A R, Coppens A B, Sanders J V, *Fundamentals of Acoustics*, 3rd Edition, John Wiley & Sons, Inc, Toronto, pp. 182 - 185, 1982.

[58] Nielsen R O, *Sonar Signal Processing*, Artech House, Inc., Chapter 2, 1991.

[59] Buckingham M J, Berkhout B V, Glegg S A L, "Acoustic daylight: Imaging the ocean with ambient noise", *Nature*, Volume 356, pp. 327 - 329, MacMillan Magazines Ltd., 1992.

[60] Prada C, Wu F, Fink M, "The iterative time reversal mirror: A solution to self-focusing in the pulse echo mode", *Journal of the Acoustical Society of America*, Volume 90, Number 2, pp. 1119 - 1129, 1991

[61] Prada C, N Lartillot, Fink M, "Selective focusing in multiple-target media: The transfer matrix method", *IEEE Ultrasonic Symposium* (Baltimore), Volume 2, pp. 1139 - 1142, 1993.

[62] Greenberg I, "Sounds impossible", *New Scientist*, Volume 156, Number 2110, pp. 36 - 39, 29 November, 1997.

[63] Cathignol D, Birer A, Nachef S, Chapelon J-Y, "Electronic beam steering of shock waves", *Ultrasound in Medicine & Biology*, Volume 21, Number 3, pp. 365 - 377, 1995.

[64] Skolnik M I, *Radar Handbook*, 2nd Edition, McGraw-Hill Publishing Company, 1990.

[65] Buckingham M J, Jones S A S, "A new shallow-ocean technique for determining the critical angle of the seabed from the vertical directionality of the ambient noise in the water column", *J. Acoust. Soc. Am.*, Vol. 81, No. 4, pp. 938 - 946, April 1987.

[66] Potter J R, "Acoustic imaging using ambient noise: Some theory and simulation results", *J. Acoust. Soc. Am.*, Vol. 95, No. 1, pp. 21 - 33, January 1994.

[67] Hecht E, *Optics*, 2nd Edition, Addison-Wesley Publishing Company, Chapter 4, pp. 87 - 92, 1987.

[68] Hecht E, *Optics*, 2nd Edition, Addison-Wesley Publishing Company, Chapter 6, p. 227, 1987.

[69] Kinsler L E, Frey A R, Coppens A B, Sanders J V, *Fundamentals of Acoustics*, 3rd Edition, John Wiley & Sons, Inc, Toronto, Chapter 5, pp. 115 - 117, 1982.

[70] Livett A J, Preston R C, "A comparison of the AIUM/NEMA, IEC and FDA (1980) definitions of various acoustic output parameters for ultrasonic transducers", *Ultrasound in Medicine and Biology*, Volume 11, Number 6, pp. 793 - 802, 1985.

[71] Ogilvy J A, *Theory of Wave Scattering from Random Rough Surfaces*, Adam Hilger, Bristol, 1991.

[72] Van Vlack L H, *Elements of Materials Science and Engineering*, Sixth Edition, Addison-Wesley Publishing Company, p. 509, 1989.

[73] Evans, R C P, "Acoustic penetration of the seabed, with particular application to the detection of non-metallic buried cables", *PhD Thesis, University of Southampton*, 1999.

[74] Evans R C. Leighton T G, "The Detection of cylindrical objects of low acoustic contrast buried in the seabed", *J. Acoust. Soc. Am.*, Vol. 103, p. 2902, 1998.

[75] Evans R C. Leighton T G, "The Detection of Cylindrical Objects of Low Acoustic Contrast Buried in the Seabed", *Proceedings of the 16th International Congress on Acoustics and 135th Meeting of the Acoustical Society of America (ICA/ASA '98)*, Edited by Kuhl P K and Crum L A, pp. 1369 - 1370, 1998.

[76] Evans R C, Leighton T G, “An experimental investigation of acoustic penetration into sandy sediments at sub-critical grazing angles”, *Proceedings of the Fourth European Conference on Underwater Acoustics*, Edited by Alippi A and Cannelli G B, pp. 697 - 702, 1998.

[77] Hecht E, *Optics*, 2nd Edition, Addison-Wesley Publishing Company, pp. 87 - 92, 1987.

[78] Hecht E, *Optics*, 2nd Edition, Addison-Wesley Publishing Company, p. 138, 1987.

[79] Hecht E, *Optics*, 2nd Edition, Addison-Wesley Publishing Company, pp. 220 - 221, 1987.

[80] Hecht E, *Optics*, 2nd Edition, Addison-Wesley Publishing Company, p. 232, 1987.